Cellular/Molecular

H3K27 Trimethylation-Mediated Downregulation of miR-216a-3p in Sensory Neurons Regulates Neuropathic Pain Behaviors via Targeting STIM1

Yufang Sun,[1,2]* Yu Tao,[2]* Junping Cao,[3]* Yaqun Zhang,[2] Zitong Huang,[2] Shoupeng Wang,[2] Weiwei Lu,[2] Qi Zhu,[2] Lidong Shan,[2] Dongsheng Jiang,[4,5] Yuan Zhang,[1,6,7] and Jin Tao[2,6,7]

[1]Department of Geriatrics, Clinical Research Center of Neurological Disease, The Second Affiliated Hospital of Soochow University, Suzhou 215004, China, [2]Department of Physiology and Neurobiology, Centre for Ion Channelopathy, Suzhou Medical College of Soochow University, Suzhou 215123, China, [3]Jiangsu Province Key Laboratory of Anesthesiology, Xuzhou Medical University, Xuzhou 221004, China, [4]Precision Research Center for Refractory Diseases, Shanghai General Hospital, Shanghai Jiao Tong University School of Medicine, Shanghai 201620, China, [5]Institute of Regenerative Biology and Medicine, Helmholtz Zentrum München, Munich 81377, Germany, [6]Jiangsu Key Laboratory of Neuropsychiatric Diseases, Soochow University, Suzhou 215123, China, and [7]MOE Key Laboratory of Geriatric Diseases and Immunology, Suzhou Medical College of Soochow University, Suzhou 215123, China

Although the therapeutic potential of microRNA-mediated gene regulation has been investigated, its precise functional regulatory mechanism in neuropathic pain remains incompletely understood. In this study, we elucidate that miR-216a-3p serves as a critical non-coding RNA involved in the modulation of trigeminal-mediated neuropathic pain. By conducting RNA-seq and qPCR analysis, we observed a notable decrease of miR-216a-3p in the injured trigeminal ganglia (TG) of male rats. Intra-TG administration of miR-216a-3p agomir or lentiviral-mediated overexpression of miR-216a-3p specifically in sensory neurons of injured TGs alleviated established neuropathic pain behaviors, while downregulation of miR-216a-3p (pharmacologically or genetically) in naive rats induced pain behaviors. Moreover, nerve injury significantly elevated the histone H3 lysine-27 (H3K27) trimethylation (H3K27me3) levels in the ipsilateral TG, thereby suppressing the SRY-box TF 10 (SOX10) binding to the *miR-216a-3p* promoter and resulting in the reduction of miR-216a-3p. Inhibiting the enzymes responsible for catalyzing H3K27me3 restored the nerve injury-induced reduction in miR-216a-3p expression and markedly ameliorated neuropathic pain behaviors. Furthermore, miR-216a-3p targeted stromal interaction molecule 1 (STIM1), and the decreased miR-216a-3p associated with neuropathic pain caused a significant upregulation in the protein abundance of STIM1. Conversely, overexpression of miR-216a-3p in the injured TG suppressed the upregulation of STIM1 expression and reversed the mechanical allodynia. Together, the mechanistic understanding of H3K27me3-dependent SOX10/miR-216a-3p/STIM1 signaling axial in sensory neurons may facilitate the discovery of innovative therapeutic strategies for neuropathic pain management.

Key words: **histone methylation; miR-216a-3p; neuropathic pain; stromal interaction molecule 1; trigeminal ganglion neurons**

Significance Statement

MicroRNA (miRNAs) are posttranscriptional regulators of gene expression that play critical roles in the pathogenesis of neuropathic pain. However, the detailed mechanisms by which most pain-associated miRNAs operate and their therapeutic potential are incompletely understood. Our present study revealed that nerve injury-induced histone H3 lysine 27 trimethylation reduces the binding of SRY-box transcription factor 10 to the promoter region of the *miR-216a-3p* gene, leading to decreased expression of the miRNA, miR-216a-3p. This reduction subsequently promotes neuropathic pain by regulating stromal interaction molecule 1. Given that miRNA-mediated gene regulation is a proposed therapeutic approach for treating neuropathic pain, our findings suggest that replenishing miR-216a-3p could serve as a novel strategy for treating chronic neuropathic pain.

Received March 27, 2024; revised Nov. 12, 2024; accepted Nov. 16, 2024.

Author contributions: Y.S., Y.Z., and J.T. designed research; Y.S., Y.T., J.C., Y.Z., Z.H., S.W., W.L., Q.Z., and L.S. performed research; Y.S., Y.T., J.C., and Y.Z. analyzed data; Y.S., D.J., Y.Z., and J.T. wrote the paper.

This work was supported by grants from the National Science Foundation for Distinguished Young Scholars of China (Grant No. 82425019), the National Natural Science Foundation of China (Grant Nos. 82071236, 82271245 and 82371218), the Clinical Research Center of Neurological Disease (Grant No. ND2022B03), the Jiangsu Key Laboratory of Neuropsychiatric Diseases (Grant No. BM2013003), the Natural Science Foundation of Jiangsu Province (Grant No. BK20211073), the Science and Technology Bureau of Suzhou (Grant No. SYS2020129), the MOE Key Laboratory of Geriatric Diseases and Immunology (Grant No. JYN202403), the State Key Laboratory of Radiation Medicine and Protection (Grant No. GZK1202223), the National Key Research and Development Program of China (Grant to Y.Z. and J.T.), and the Priority Academic Program Development of Jiangsu Higher Education Institutions (Grant No. PAPDJHEI).

*Y.S., Y.T., and J.C. contributed equally to this work.

The authors declare no competing financial interests.

Correspondence should be addressed to Jin Tao at taoj@suda.edu.cn or Yuan Zhang at yuanzhang@suda.edu.cn.

https://doi.org/10.1523/JNEUROSCI.0607-24.2024

Introduction

Neuropathic pain is a type of chronic pain that occurs as a result of dysfunction or damage to the nerves and has a profound impact on an individual's daily life, affecting their physical abilities and overall quality of life (Baron et al., 2010). However, to date, the treatment of neuropathic pain has faced challenges, with limited success achieved so far. Current medications, like opioids and nonsteroidal anti-inflammatory drugs, offer only modest pain relief and can come with severe side effects, including addiction (Finnerup et al., 2021). Thus, elucidating the underlying mechanisms that contribute to neuropathic pain is crucial to discover preventative strategies and innovative treatments and preventive strategies for this condition. Studies focusing on first-order sensory neurons, including trigeminal ganglion neurons, have revealed that peripheral nerve injury can lead to alterations in the expression of pain-associated genes at both the transcriptional and translational levels (Kogelman et al., 2017; Korczeniewska et al., 2020). These alterations possess significant genomic signatures and regulatory mechanisms and play critical roles in the onset and persistence of neuropathic pain and that represent pivotal targets for analgesic interventions in the management of neuropathic pain (Messlinger and Russo, 2019; Kc et al., 2022). Therefore, understanding how these pain-related molecules/genes are altered in the injured trigeminal ganglia (TG) may offer new therapeutic targets for neuropathic pain treatment.

MicroRNAs (miRNAs) are short, noncoding RNA molecules that typically consist of 21–25 nucleotides in their mature form. They play pivotal roles in the regulation of gene expression by directly binding to the 3′-UTR of mRNAs of target genes and thereby to downregulate the protein expression levels posttranscriptionally (Rupaimoole and Slack, 2017). Studies have highlighted the involvement of miRNA-mediated modulation in a wide range of diseases, leading to the exploration of miRNA-based therapeutics as a potential treatment strategy (Bartel, 2009). Consequently, both preclinical and clinical trials evaluating miRNA-based therapeutics have been initiated to investigate the potential of miRNAs in disease treatment (John et al., 2004). MiR-216a-3p, in particular, has been shown to be abundant and highly conserved across different species. This miRNA has been demonstrated to modulate various biological processes, including the inflammatory response (Ni et al., 2023) and cell apoptosis and diseases, including chronic pancreatitis (Liu et al., 2019) and lung cancer (Tang et al., 2020). While limited evidence demonstrates a potential regulatory role in nervous system disorders, miR-216a-3p has been recently shown to regulate Bcl-2-associated X protein and is involved in Parkinson's disease (Wang et al., 2021). Nevertheless, it remains to be determined whether and how miR-216a-3p in sensory neurons participates in regulating nociceptive responses.

In this study, we have identified miR-216a-3p as a pivotal noncoding RNA in sensory neurons that is involved in the maintenance and development of neuropathic pain. We found that nerve injury leads to increased methylation of histone H3 lysine-27 (H3K27), which prevents the SRY-box transcription factor (TF) 10 (SOX10) binding to the *miR-216a-3p* promoter, leading to a decreased expression level of miR-216a-3p. Furthermore, we also found that the decreased miR-216a-3p levels contribute to neuropathic pain by targeting stromal interaction molecule 1 (STIM1), an ER-intraluminal Ca^{2+} sensor that regulates store-operated Ca^{2+} entry (SOCE) and Ca^{2+} mobilization and contributes to cellular exocytosis related to pain symptoms. Our findings highlight the critical role of the sensory H3K27 trimethylation (H3K27me3)/SOX10/miR-216a-3p/STIM1 signaling axis in regulating neuropathic pain behaviors. This in-depth mechanistic understanding may provide valuable insights for the development of innovative therapeutic targets for the management of neuropathic pain.

Materials and Methods

Animal model and behavioral tests. The Institutional Animal Care and Use Committee of Soochow University had given its approval to all experimental procedures, which were carried out in compliance with the National Institutes of Health guidelines for animal research and the International Association for the Study of Pain. Adult Sprague Dawley rats (male, 8–10 weeks) were housed in a temperature- and humidity-controlled facilities on a 12/12 h light/dark cycle with food and water available *ad libitum*. Every effort was made to minimize suffering and the number of animals used. As described previously (Martin and Avendano, 2009; Qi et al., 2022), chronic constriction injury (CCI) of the infraorbital nerve (CCI-ION) was used to establish an animal model of trigeminal neuropathic pain. In short, after the animal is anesthetized with isoflurane, a small incision is made near the left ION. The left ION was dissected close to the IOF after isoflurane anesthesia. The ION was carefully separated from the surrounding tissue with a blunt curved glass rod, and two silk ligatures were tied loosely around the ION with 4–0 chromic guts (∼2 mm apart). The ION of sham animals was exposed using the same surgical procedure except for ligation.

All behavioral experiments were performed in double-blind conditions. Orofacial behavioral assessments were conducted 1 d before and at predetermined times following CCI-ION surgery. One rat was placed in each cage and the experiment began after 2 h of acclimatization. The von Frey filament (Ugo Basile) started with a minimum stimulus intensity of 0.008 g and tested gradually toward a maximum stimulus intensity of 15 g (Stoelting), stimulating the region of the left vibrissa pad skin of the face. Each stimulus filament was applied three times consecutively with an interval of ∼2 s between each test as previously described (Wang et al., 2019; Zhang et al., 2021; Qi et al., 2022). To avoid tissue injury and head rotation due to excessive mechanical force in rats, we set a cutoff point of 15 g filament. The escape threshold was tested with a graded series of calibrated von Frey filaments in a sequential ascending force until positive nociceptive behavior occurred. As described by Vos et al. (1994) and in our previous studies (Qi et al., 2022), these positive responses to mechanical stimulation included a rapid head withdrawal behaviors or attack/escape reactions. The minimal force applied through von Frey filaments to trigger at least one of these behaviors was considered as the mechanical response threshold. Heat sensitivity, expressed as head withdrawal latency, was tested by radiant heat using the Hargreaves apparatus (Ugo Basile) as previously described (Kopruszinski et al., 2015; Zhang et al., 2021). The intensity of the radiant heat was adjusted to yield a basal latency between 8 and 12 s, with a cutoff latency of 18 s to avoid tissue damage.

Drug application. A percutaneous approach for injecting the trigeminal ganglion (intra-TG injection) was conducted as described previously (Qi et al., 2022). Briefly, a microinjection needle was inserted through the infraorbital foramen (IOF), infraorbital canal, and foramen rotundum. The needle tip terminated at the medial part of the TG. An injection volume of 3 μl was slowly delivered (over a 5 min period), and 10 min of needle retention was applied before the needle was removed. The 5′-cholesteryl-modified and 2′-O-methyl-modified small–interfering RNA (siRNA) for STIM1 (STIM1-siRNA), agomir-216a-3p, antagomir-216a-3p, or appropriate scrambled controls (RiboBio Technology), tagged with Cy3, were diluted in DEPC-H_2O. Neuron promoter-specific (human synapsin 1 gene promoter, hSyn) combinatorial lentiviral vectors carrying the enhanced green fluorescent protein (EGFP) gene, including lenti-hSyn-miR-216a-3p-up (miR-216a-up), lenti-hSyn-miR-216a-3p-antisense (miR-216a-AS), lenti-hSyn-STIM1-up (STIM1-up), and the

appropriate negative controls, were obtained from GeneChem. The agomir, antagomir, or siRNA sequences are summarized in Table 1.

Western blot analysis. Western blot analysis was conducted as described in our previous studies (Zhang et al., 2014; Wang et al., 2019). Briefly, equal amounts of protein (30 μg) were loaded, separated by sodium dodecyl sulfate-polyacrylamide gel electrophoresis at 10% (for SOX10 and STIM1 proteins) or 12% (for H3K9me2 and H3K27me3 proteins) and electroblotted onto polyvinylidene fluoride membranes (Merck Millipore). After blocking in 5% skim milk, the blots were incubated with primary antibodies against STIM1 (rabbit, 1:1,000, Cell Signaling Technology), SOX10 (rabbit, 1:1,000, Proteintech), H3K27me3 (mouse, 1:800, Abcam), H3K9me2 (mouse, 1:800, Abcam), H3 (rabbit, 1:1,000, Abcam), or GAPDH (rabbit, 1:3,000, Abcam). The blots were washed and then incubated with horseradish peroxidase-conjugated goat anti-rabbit (1:5,000, Cell Signaling Technology) or goat anti-mouse (1:5,000, Cell Signaling Technology) secondary antibodies. Bands were visualized with SuperSignal West Pico PLUS (Thermo Fisher Scientific). The Quantity One software was used for image analysis after they were taken using the ChemiDoc XRS system (Bio-Rad Laboratories). GAPDH and H3 were used as loading controls to normalize the amounts of proteins.

Immunofluorescence staining. A standard protocol of immunostaining was performed as described in our previous studies (Cao et al., 2019; Qi et al., 2022). In brief, TGs were rapidly dissected, postfixed in 4% PFA, cryoprotected in 15–30% sucrose, and then sectioned into 15 μm slices on a cryostat (CM1950, Leica Microsystems). TG slices were permeabilized with 0.15% Triton X-100 for 30 min, blocked with 5% normal goat serum in phosphate buffer saline for 1 h, and then incubated overnight at 4°C with primary antibodies against STIM1 (rabbit, 1:500; Cell Signaling Technology), NeuN (mouse, 1:500, Abcam), GS (mouse, 1:500, Abcam), NF-200 (mouse, 1:500, Abcam), CGRP (mouse, 1:500, Abcam), H3K27me3 (mouse, 1:500, Abcam), and SOX10 (rabbit, 1:500, Proteintech). The sections were then visualized with IB4-fluorescein isothiocyanate (5 μg/ml; Sigma-Aldrich) and Alexa Fluor 555- or Alexa Fluor 488-conjugated secondary antibodies (1:300, Cell Signaling Technology). Images were captured under an upright fluorescence microscope (Nikon 104C) with a CoolSnap HQ2 CCD camera (Photometrics).

Fluorescence in situ hybridization (FISH). FISH was conducted following the procedure as described previously (Tao et al., 2023). Locked nucleic acid-specific probes conjugated with digoxigenin (DIG) for miRNA-216a-3p were obtained from Exon (Guangzhou Exon Technology). In miRNA hybridization buffer, the probe rno-miR-216a-3p (5′-DIG-CATAATCCCAGAGACCACTGTG-DIG-3′) was denatured and stabilized. Following hybridization, the sections underwent rinsing, blocking, and incubation with anti-digoxin antibody (1:150) that was Cy3-labeled. For the colabeling experiments, TG sections were first hybridized with the miRNA-216a-3p probe and then were incubated with antibodies against STIM1 (rabbit, 1:500, Cell Signaling Technology), GS (mouse, 1:500, Abcam), NeuN (mouse, 1:500, Abcam), SOX10 (rabbit, 1:500, Proteintech), or H3K27me3 (mouse, 1:500, Abcam), followed by detection using an Alexa Fluor 488-conjugated goat anti-mouse (1:300) or anti-rabbit (1:300) IgG antibodies (both from Cell Signaling Technology). Fluorescent images were obtained using a fluorescence microscope as described above.

Table 1. Agomir, antagomir, siRNAs, and probes used in the current study

Name	Sense	Antisense
rno-miR-216a-3p agomir	CACAGUGGUCUCUGGGAUUAUG	UAAUCCCAGAGACCACUGUGUU
Agomir-NC	UUCUCCGAACGUGUCACGUTT	ACGUGACACGUUCGGAGAATT
rno-miR-216a-3p antagomir	CAUAAUCCCAGAGACCACUGUG	
Antagomir-NC	CAGUACUUUUGUGUAGUACAA	
rno-miR-216a-3p mimics	CACAGUGGUCUCUGGGAUUAUG	UAAUCCCAGAGACCACUGUGUU
Mimics NC	UUCUCCGAACGUGUCACGUTT	ACGUGACACGUUCGGAGAATT
siRNA-stim1	GGGAAGACCUCAAUUACCADTDT	UGGUAAUUGAGGUCUUCCCDTDT
siRNA-NC	UUCUCCGAACGUGUCACGUTT	ACGUGACACGUUCGGAGAATT
rno-miR-216a-3p FISH probe	CATAATCCCAGAGACCACTGTG	

PCR, RT-PCR, and real-time quantitative PCR. Total RNA was extracted from the rat TG using Takara RNAiso Plus as described previously (Qi et al., 2022). Purified RNAs were reverse-transcribed by the PrimeScript RT Reagent Kit (Takara Bio) to obtain complementary DNA (cDNA). Subsequently, cDNA was analyzed by endpoint PCR (PCR) or quantitative real-time PCR (qPCR), respectively. PCR was performed via the Eppendorf Mastercycler nexus GSX1 System with PrimeSTAR Max DNA Polymerase (Takara Bio). The reactions were carried out for 35 cycles (denaturation at 94°C for 15 s, annealing at 60°C for 30 s, extension at 72°C for 30 s) preceded by 3 min denaturation at 94°C and followed by 5 min extension at 72°C. The specificity of the amplified PCR product was verified by agarose gel electrophoresis. qPCR was conducted using the ROCHE LightCycler 96 System with SYBR Green qPCR Master Mix (Takara Bio) and verified by melting-curve analysis. The quantification of miRNA was conducted using the $2^{-\Delta\Delta Cq}$ method, with the internal control U6 employed for normalization. The primers of PCR and qPCR are summarized in Tables 2 and 3.

Ca^{2+} imaging. Primary cultured rat TG neurons were prepared for calcium imaging by incubating them overnight. The neurons were loaded with 2 μM Fura-2 AM (Invitrogen) for 30 min at 37°C in a humidified 5% CO_2 incubator, followed by a 30 min wash in Ca^{2+}-free Hanks Balanced Salt Solutions (HBSS) at room temperature. After a 2 min baseline measurement, 2 μM thapsigargin (MedChemExpress, in Ca^{2+}-free HBSS) was introduced. After 5 min, The HBSS buffer containing 1.5 mM $CaCl_2$ was perfused using a custom valve control system. Imaging was performed using a 100× objective, capturing cells at dual excitation wavelengths of 340 and 380 nm, with detection at 510 nm, along with background correction and F340/F380 ratio calculations. A CCD camera (PCO) attached to an inverted microscope (Nikon) was used for image acquisition, with Fura-2 excitation provided by an alternating light source (Photon Technology International) emitting at 340 and 380 nm.

Dual-luciferase reporter assay. Luciferase reporter assay was conducted as previously described (Qi et al., 2022). The different truncated regions of the *miR-216a-3p* promoter (−2,010 to 0 bp) were amplified by PCR and then respectively inserted into the pGL3-basic luciferase reporter plasmid (Promega) using HindIII and XhoI endonuclease to construct a series of plasmids (pGL3-F1 to pGL3-F5). JASPAR (http://jaspar.genereg.net/) was used to predict the potential binding sites on the Δ*F* region in the *miR-216a-3p* promoter (−448 to 0 bp) for SOX10. Sequences containing wild-type (miR-216a-wt) or mutant of SOX10-binding sites (miR-216a-mut) in the full-length Δ*F* of *miR-216a-3p* promotor were constructed. Either the full-length wild–type (STIM1-wt) or mutant (STIM1-mut) 3′-UTR of the STIM1 mRNA containing the putative miR-216a-3p binding sites was amplified by PCR and cloned into the pGL3-control plasmid (Promega). Both STIM1-wt and STIM1-mut were introduced downstream of the firefly luciferase gene into the pGL3-control plasmid. GeneWiz developed each construct, and all cloned constructs were subsequently confirmed by Sanger sequencing (GeneWiz). For data normalization, pGMR-TK containing Renilla luciferase was cotransfected with pGL3. The STIM1-wt (500 ng) or STIM1-mut (500 ng), together with pGMR-TK (100 ng) and miR-216a-3p mimics (or the negative control, 500 ng) were cotransfected into HEK293T cells using Lipofectamine 6000 (Invitrogen). Similar to this, Lipofectamine 6000 (Invitrogen) was used to transfect the miR-216a-wt (500 ng) or miR-216a-mut (500 ng), together with pGMR-TK (100 ng) and SOX10 overexpression plasmids pcDNA-SOX10 (or the negative control, 500 ng) into PC12 cells. A Dual-Glo Luciferase Assay System (Promega) was used to evaluate

Table 2. Primers of miRNAs used in the current study

Name	RT	Forward	Reverse
miR-216a-3p	GTCGTATCCAGTGCAGGGTCCGAGGTATTCGCACTGGATACGACCATAAT	AAGCGACCCACAGTGGTCTCT	ATCCAGTGCAGGGTCCGAGG
miR-129-5p	GTCGTATCCAGTGCAGGGTCCGAGGTATTCGCACTGGATACGACGCAAGC	AACAGACTTTTTGCGGTCTGG	
miR-181b-1-3p	GTCGTATCCAGTGCAGGGTCCGAGGTATTCGCACTGGATACGACTTGCAT	AACACGTGCTCACTGAACAATG	
miR-217-5p	GTCGTATCCAGTGCAGGGTCCGAGGTATTCGCACTGGATACGACCCAGTC	AACAGTGTACTGCATCAGGAACT	
miR-216b-5p	GTCGTATCCAGTGCAGGGTCCGAGGTATTCGCACTGGATACGACTCACAT	AACAAGAAATCTCTGCAGGCAA	
miR-216a-5p	GTCGTATCCAGTGCAGGGTCCGAGGTATTCGCACTGGATACGACTCACAG	AACAGTGTAATCTCAGCTGGCA	
U6	GTCGTATCCAGTGCAGGGTCCGAGGTATTCGCACTGGATACGACAAAATA	AGAGAAGATTAGCATGGCCCCTG	

Table 3. Sequences of nucleotides used in the current study

Name	Forward	Reverse
CHIP	CTGCGCATCTGCGAGGT	GCCAAAACCCAAAGGCTTCC
S1	GGGGTACCACCAGGTAGGAGAAA	CCGCTCGAGTGCCTAAGCCAGTA
S2		CCGCTCGAGTGTGAAGCAGTGGC
S3		CCGCTCGAGAGTGGGACTGCTATT
S4		CCGCTCGAGGTGACGAGGAACATC
S5		CCGCTCGAGGGACCTGCAAGAAA

the firefly and Renilla luciferase activity 48 h after transfection. First, after treatment with the Dual-Glo luciferase reagent, the activity of firefly luminescence was evaluated. Next, Dual-Glo Stop and Glo reagents were added to each well to measure Renilla luciferase activity. The luminescence of firefly luciferase was normalized according to the corresponding Renilla luciferase activity.

Chromatin immunoprecipitation (ChIP)-qPCR. ChIP-qPCR was conducted as described in our previous studies (Tao et al., 2023). Briefly, the SimpleChIP Plus Enzymatic Chromatin IP kit was used to prepare samples for ChIP assays (Cell Signaling Technology). Rat TGs were dissected and finely minced in phosphate-buffered saline containing a protease inhibitor cocktail. The nuclear tissues were then subjected to digestion using micrococcal nuclease for 20 min at a temperature of 37°C. This process aimed to generate short DNA fragments with lengths typically ranging from 150 to 500 bp. The specimens were precipitated and separated by a high-speed centrifugation and then sonicated in ChIP buffer and underwent a 10 min centrifugation at 9,500 rpm and 4°C to collect the supernatant containing DNA fragments. Two percent of the supernatant (from the previous step) served as the DNA input control, and the rest of the samples were subjected to slow spinning to precipitate and pull down chromatin at 4°C overnight after being treated with H3K27me3 (Abcam), SOX10 (Proteintech), or IgG (negative control, Cell Signaling Technology). To capture the immunoprecipitated complexes, ChIP-grade protein G magnetic beads (Cell Signaling Technology) were utilized. Proteinase K was used to break down the cross-links created by protein and DNA, and DNA purification columns were used to separate the DNA. Part of the immunoprecipitated DNA samples were used to performed endpoint PCR, and PCR products were separated by 2% agarose gel electrophoresis and visualized using UV light to assess the specificity of the amplicon. The remaining immunoprecipitated DNA samples were submitted to a real-time qPCR experiment using the following target promoter-specific primers (forward, 5′-CTGCGCATCTGCGAGGT-3′, and reverse, 5′-GCCAAAACCC AAAGGCTTCC-3′). Values for the miR-216a-3p promoter's enrichment were normalized to input DNA values, and these values of experimental group were subsequently normalized to the enrichment of the control group. PCR products were separated by 2% agarose gel electrophoresis and visualized using UV light.

Electrophysiology. Whole-cell patch–clamp recordings were conducted at room temperature (23 ± 1°C) as described previously (Huang et al., 2024). TG neurons were recorded 3–6 h after plating. Current measurements were made using a MultiClamp 700B amplifier (Molecular Devices). The signals were filtered with a low-pass filter at 2 kHz and digitized at a sampling rate of 10 kHz using a Digidata 1440 A digitizer (Molecular Devices). Data acquisition was performed with a pClamp10 software (Molecular Devices), and the collected data were analyzed using Clampfit 10.2 (Molecular Devices). Patch pipettes (World Precision Instruments) had resistances of 3–5 MΩ when filled with the internal solution. For current-clamp recordings, the intracellular pipette solution contained the following (in mM): 110 KCl, 25 HEPES, 10 NaCl, 0.3 Na-GTP, 4 Mg-ATP, and 2 EGTA, pH 7.4 adjusted with KOH (295 mOsm). The extracellular solution contained the following (in mM): 128 NaCl, 2 KCl, 2 $CaCl_2$, 2 $MgCl_2$, 25 HEPES, and 30 glucose, pH 7.4 adjusted with NaOH (305 mOsm). The retrograde tracer DiI (20 mg/ml, Thermo Fisher Scientific) was injected subcutaneously into the whisker pads of the rats. Four days postinjection, small TG neurons (soma diameter, <30 μm) were patch-clamp recorded.

Data analysis and statistics. The data in the study are expressed as the mean ± SEM. The data acquisition and statistical analysis were conducted using Clampfit 10.2 (Molecular Devices), Microsoft Excel, and Prism 7.0 (GraphPad Software). To determine the significance between two groups, a two-tailed Student's *t* test was used. One-way ANOVA with Bonferroni's post hoc test was used for comparisons between multiple groups with a single variable. For comparisons involving multiple variables, a two-way repeated-measure ANOVA followed by Bonferroni's test was utilized. Statistical significance was defined as $p < 0.05$. Differences with a *p* value below this threshold were considered statistically significant.

Results

miR-216a-3p is downregulated in TG neurons after peripheral nerve injury

Unilateral CCI-ION was utilized to establish the animal model of trigeminal neuropathic pain. Compared with the sham groups, rats with CCI-ION exhibited a significant reduction in the mechanical pain threshold for escape behavior on Day 14 and maintained at least Postoperative Day 28 (Fig. 1*A*; two-way ANOVA; for Days 14, 21, and 28; $p = 0.0001$). To identify crucial miRNAs as well as their regulatory networks that contribute to trigeminal neuropathic pain, we conducted RNA sequencing analysis on the TG samples at 14 d post-CCI-ION [Gene Expression Omnibus (GEO) accession number GSE192803]. Among the top 20 miRNAs with a notably decreased expression (Fig. 1*B*), only six miRNAs were identified as highly conserved in humans and rats (Fig. 1*C*). Further qPCR analysis confirmed that miR-216a-3p was most significantly downregulated in the CCI-ION rats (Fig. 1*C*; Student's *t* test; for miR-181b-1-3p, $p = 0.0228$; for miR-216a-3p, $p = 0.0001$; for miR-547-5p, $p = 0.0004$; for miR-217-5p, $p = 0.0099$). As a result, we decided to examine the expression and functional characteristics of miR-216a-3p. We observed a significant abundance of the miR-216a-3p transcript within the TG by PCR analysis (Fig. 1*D*; Extended Data Fig. 1-1). Furthermore, qPCR measurement revealed that its expression level in the TG was significantly elevated compared with that in the brain (~5.7-fold higher; Fig. 1*E*; Student's *t* test; $p = 0.0027$). Afterward, we examined

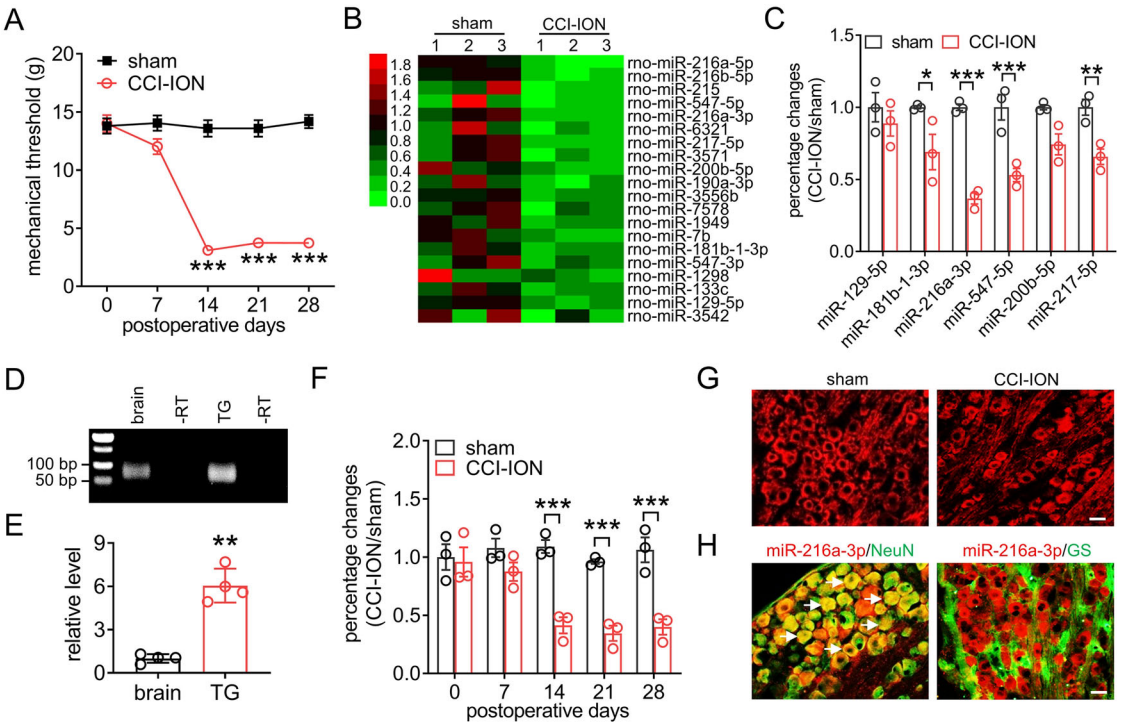

Figure 1. miR-216a-3p is downregulated in TG neurons following nerve injury. ***A***, Escape threshold in CCI-ION operation or sham surgery. ***$p < 0.001$ (vs sham), by two-way ANOVA. $n = 8$ rats/group. ***B***, Heatmap of the top twenty miRNAs downregulated in the injured TG at 14 d following CCI-ION. ***C***, Expression levels of six highly conserved miRNAs in the injured TG at 14 d following CCI-ION operation or sham surgery. *$p < 0.05$, **$p < 0.01$, and ***$p < 0.001$ (vs sham), by Student's *t* test. $n = 6$ rats/group. ***D***, ***E***, RT-PCR analysis (***D***) and real-time quantitative PCR validation (***E***) of miR-216a-3p expression in the TG and brain of intact rats. **$p < 0.01$ (vs brain), by Student's *t* test. $n = 4$ rats/group. Also see Extended Data Figure 1-1. ***F***, Time course of miR-216a-3p expression in CCI-ION operation or sham surgery. ***$p < 0.001$ (vs sham), by two-way ANOVA. $n = 6$ rats/group. ***G***, RNA FISH analysis of miR-216a-3p in the injured TG 14 d following CCI-ION operation or sham surgery. Scale bar, 50 µm. ***H***, RNA FISH analysis of miR-216a-3p combined with immunofluorescence labeling of NeuN and GS. Colocalizations are indicated by white arrows. Scale bar, 50 µm.

the time course of miR-216a-3p expression in the ipsilateral TG following nerve injury. Our qPCR analysis revealed a notable decrease in miR-216a-3p expression levels on Day 14, which remained reduced for at least 28 d in CCI-ION rats (Fig. 1*F*; two-way ANOVA; for Day 14, $p = 0.0001$; for Day 21, $p = 0.0002$; for Day 28, $p = 0.0001$). No significant differences were observed in sham groups at any time point (Fig. 1*F*). Subsequently, we examined the cellular distribution of miR-216a-3p within the TG. RNA FISH revealed the basal expression of miR-216a-3p in small- and medium-sized TG neurons, which was decreased at 14 d following CCI-ION operation (Fig. 1*G*). Moreover, FISH combined with immunofluorescence staining (immunoFISH) analysis demonstrated that miR-216a-3p was predominantly coexpressed with the neuronal marker NeuN while showing rare colocalization with the satellite glial cell marker GS (Fig. 1*H*), indicating that miR-216a-3p is primarily expressed in neurons within the rat TGs.

miR-216a-3p regulates trigeminal-mediated nociceptive behaviors

To verify that whether miR-216a-3p participated in trigeminal neuropathic pain, we unilaterally injected an agomir of miR-216a-3p (agomir-216a) into the injured TG at 14 d following CCI-ION. At 1–3 d after administration, agomir-216a dramatically attenuated mechanical allodynia induced by CCI-ION operation, while the treatment of agomir-NC did not elicit such effects (Fig. 2*A*; two-way ANOVA; for Days 0, 1, 2, and 3, $p = 0.0001$; CCI-ION + agomir-NC vs sham + antagomir-NC; for Day 2 and 3, $p = 0.0001$; CCI-ION + agomir-216a vs CCI-ION + antagomir-NC). Moreover, we utilized a lentiviral-mediated approach to induce miR-216a-3p expression specifically in TG neurons under a neuron-specific promoter, lenti-hSyn-miR-216a-3p-up (miR-216a-up), which contained an eGFP construct serving as an expression marker. The GFP expression started to be detected at 3 d following intra-TG injection and lasted for at least 21 d (Fig. 2*B*; Extended Data Fig. 2-1*A*,*B*). Similarly, we observed a significant increase in miR-216a-3p expression at 3 d after administration of miR-216a-up (Fig. 2*C*; Student's *t* test; $p = 0.0024$). Moreover, intra-TG injection of miR-216a-up at 14 d after CCI-ION resulted in a substantial alleviation of mechanical allodynia from Day 3 to Day 7 after drug administration (Fig. 2*D*; two-way ANOVA; for Days 0, 3, and 7, $p = 0.0001$; CCI-ION + miR-NC vs sham + miR-NC; for Days 3 and 7, $p = 0.0001$; CCI-ION + miR-216a-up vs CCI-ION + miR-NC). To further investigate the role of miR-216a-3p in the development of trigeminal-mediated neuropathic pain, we evaluated the effect of preinjection of miR-216a-3p-up before CCI-ION operation. Compared with sham surgery, the preinjection of miR-216a-3p-up significantly ameliorated nerve injury-induced mechanical allodynia at 14 d after surgery (Fig. 2*E*; two-way ANOVA; for Days 14 and 21, $p = 0.0001$; miR-NC + CCI-ION vs miR-NC + sham; for Days 14 and 21, $p = 0.0001$; miR-216a-up + CCI-ION vs miR-NC + CCI-ION). Additionally, we conducted experiments to explore whether mimicking the nerve injury-induced downregulation of miR-216a-3p in TG neurons of intact rats would impact nociceptive thresholds. The unilateral administration of miR-216a-3p antagomir (antagomir-216a) resulted in the

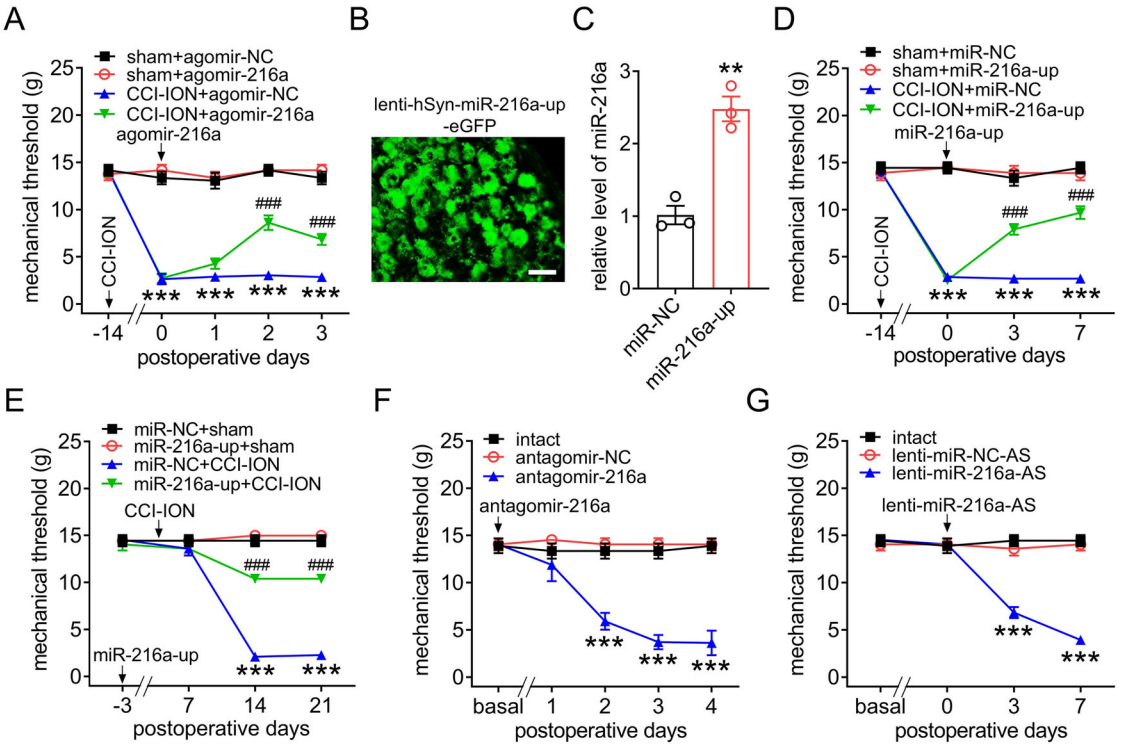

Figure 2. miR-216a-3p regulates neuropathic pain behaviors in rats. ***A***, Effect of agomir-216a or agomir-NC on mechanical allodynia on Day 14 after CCI-ION operation or sham surgery. ***$p < 0.001$ (vs sham + antagomir-NC); $^{###}p < 0.001$ (vs CCI-ION + antagomir-NC); by two-way ANOVA. $n = 7$ rats/group. ***B***, Images of eGFP-expressing TG neurons after administration of lenti-hSyn-miR-216a-3p-up-eGFP (miR-216a-up) on Day 3. Scale bar, 50 µm. Also see Extended Data Figure 2-1, *A* and *B*. ***C***, The expression level of miR-216a-3p after intra-TG injection of miR-216a-up or miR-NC. **$p < 0.01$ (vs miR-NC), by Student's *t* test. $n = 6$ rats/group. ***D***, Effect of miR-216a-up or miR-NC on mechanical allodynia at 14 d after CCI-ION operation or sham surgery. ***$p < 0.001$ (vs sham + miR-NC); $^{###}p < 0.001$ (vs CCI-ION + miR-NC); by two-way ANOVA. $n = 8$ rats/group. ***E***, Effect of preadministration of miR-216a-up or miR-NC on the CCI-ION-induced decrease in the mechanical threshold. ***$p < 0.001$ (vs miR-NC + sham); $^{###}p < 0.001$ (vs miR-NC + CCI-ION); by two-way ANOVA. $n = 7$ rats/group. ***F***, Effect of antagomir-216a or antagomir-NC on mechanical pain hypersensitivity in intact rats. ***$p < 0.001$ (vs antagomir-NC), by two-way ANOVA. $n = 8$ rats/group. ***G***, Effect of lenti-hSyn-miR-216a-3p-antisense (lenti-miR-216a-AS) or lenti-miR-NC-AS administration on mechanical pain hypersensitivity in intact rats. ***$p < 0.001$ (vs lenti-miR-NC-AS), by two-way ANOVA. $n = 7$ rats/group.

induction of mechanical hypersensitivity on the ipsilateral side (Fig. 2*F*; two-way ANOVA; for Days 2, 3, and 4, $p = 0.0001$; antagmir-216a vs antagomir-NC). In contrast, the administration of the negative control (antagomir-NC) did not elicit a similar response. In addition, we utilized a lentiviral vector with neuron-specific promoters, lenti-hSyn-miR-216a-3p-antisense (lenti-miR-216a-AS), to study the effect of miR-216a-3p blockade on nociceptive behaviors. Intra-TG administration of lenti-miR-216a-AS in intact rats resulted in significant induction of mechanical hypersensitivity starting on Day 3, and this hypersensitivity persisted for >7 d (Fig. 2*G*; two-way ANOVA; for Days 3 and 7, $p = 0.0001$; lenti-miR-216a-AS vs lenti-miR-NC-AS). In contrast, the lenti-miR-NC-AS treatment did not induce any significant alterations in nociceptive behaviors (Fig. 2*G*).

The transcriptional factor SOX10 is responsible for miR-216a-3p transcription

To elucidate TFs responsible for regulating miR-216a-3p expression, we conducted promoter deletion analysis of the *miR-216a-3p* gene from position −2,010 to 0 bp and generated constructs of pGL3 luciferase reporter plasmids that contained different fragments of the *miR-216a-3p* promoter region (pGL3-F1 to pGL3-F5; Fig. 3*A*). Analyses of luciferase activities revealed a significant decrease in the pGL3-F2 construct (−2,010 to −448 bp) compared with pGL3-F1 (−2,010 to 0 bp), while no significant difference was observed between the other two adjacent fragments (Fig. 3*B*; Student's *t* test; $p = 0.0001$; pGL3-F1 vs pGL3-F2). These findings suggested that the fragment ranging from −448 to 0 bp (referred to as ΔF) might harbor essential *cis*-regulatory elements responsible for miR-216a-3p expression. By utilizing the JASPAR database (http://jaspar.genereg.net), we identified the TF SOX10 as the sole potential TF exhibiting binding sites within the Δ*F* region of the *miR-216a-3p* promoter. To further investigate the functional interaction between SOX10 and the Δ*F* region, we constructed a luciferase reporter construct, miR-216a-mut, with mutations in the SOX10-binding sites (Fig. 3*C*). Cotransfection of SOX10 with miR-216a-mut resulted in a significant reduction in luciferase activity compared with the wild-type group (miR-216a-wt; Fig. 3*C*; Student's *t* test; $p = 0.0001$; miR-216a-wt + SOX10 vs miR-216a-wt + control; $p = 0.0001$; miR-216a-wt + SOX10 vs miR-216a-mut + SOX10). Additionally, immunoFISH analysis showed a strong colocalization of SOX10 with miR-216a-3p in rat TG neurons, with SOX10 predominantly detected in the nuclei and miR-216a-3p mainly located in the cytoplasm (Fig. 3*D*). Surprisingly, immunoblot analysis of TG lysates did not show a significant difference in SOX10 protein expression between the CCI-ION and sham-operated groups (Fig. 3*E*; Extended Data Fig. 3-1*A*; Student's *t* test; $p = 0.6775$). Therefore, we hypothesized that the altered expression of miR-216a-3p observed in CCI-ION conditions might be attributed to changes in the binding of SOX10 to the *miR-216a-3p* promoter. Indeed, ChIP-PCR assays revealed that a *miR-216a-3p*

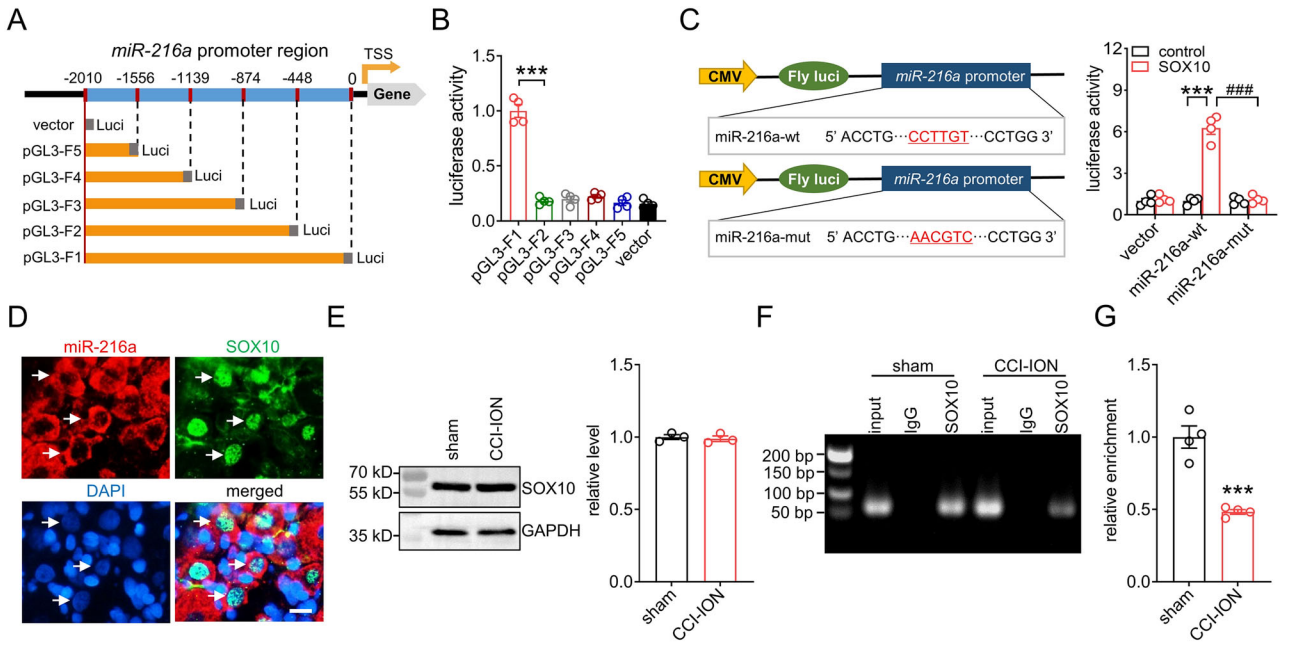

Figure 3. SOX10 activates miR-216a-3p transcription. ***A***, Schematic diagrams present different constructs of pGL3 luciferase reporters containing various fragments of the miR-216a-3p gene promoter (pGL3-F1 to pGL3-F5). ***B***, Transcriptional activities of different constructs of pGL3 luciferase reporters (pGL3-F1 to pGL3-F5) as mentioned in panel ***A***. ***$p < 0.001$ (vs pGL3-F1), by Student's *t* test. The data shown represent the mean ± SEM of four independent experiments. ***C***, Left panel, Schematic diagrams of luciferase reporter constructs containing wild-type (miR-216a-wt) or mutant SOX10-binding sites within the Δ*F* region (position −448 to 0 bp) of the *miR-216a-3p* promoter (miR-216a-mut). Right panel, Summary data demonstrating luciferase activities of miR-216a-wt and miR-216a-mut after transfection with SOX10. ***$p < 0.001$ (vs miR-216a-wt + control), $^{\#\#\#}p < 0.001$ (vs miR-216a-mut + SOX10), by Student's *t* test. The data shown represent the mean ± SEM of four independent experiments. ***D***, FISH analysis of miR-216a-3p combined with immunofluorescence labeling of SOX10 and DAPI in intact TGs. Colocalizations are indicated by white arrows. Scale bar, 25 µm. ***E***, Protein abundance of SOX10 in the injured TG at 14 d following CCI-ION operation or sham surgery. Shown blots are representative of three independent experiments. GAPDH was used as a loading control to normalize the protein abundance. $n = 6$ rats/group. Also see Extended Data Figure 3-1*A*. ***F***, ***G***, Chromatin immunoprecipitation assays were performed in TGs at 14 d post-CCI-ION or sham surgery using an antibody against SOX10. The immunoprecipitated DNA was subjected to ChIP-PCR assay (***F***) and quantitative ChIP-qPCR validation (***G***). Data were normalized to their respective input DNA and then compared with the sham groups. ***$p < 0.001$ (vs sham), by Student's *t* test. $n = 4$ rats/group. Also see Extended Data Figure 3-1*B*.

promoter fragment containing the binding motif was amplified with the complex immunoprecipitated with the SOX10 antibody (Fig. 3*F*; Extended Data Fig. 3-1*B*). On Day 14 after CCI-ION, qPCR analysis revealed that the *miR-216a-3p* promoter region exhibited a decreased occupancy of SOX10 compared with that observed after sham surgery (Fig. 3*G*; Student's *t* test; $p = 0.0006$).

H3K27 methylation decreases the binding of SOX10 to miR-216a-3p promoter

Epigenetic regulation of gene expression involves DNA methylation and histone modifications, two key mechanisms that interfere with the binding of TFs (Hamm and Costa, 2015). However, no CpG islands were identified within the Δ*F* region of the *miR-216a-3p* promoter by analyzing with MethPrimer (https://www.urogene.org/methprimer/index.html; Extended Data Fig. 4-1*A*), indicating that DNA methylation is unlikely to participate in any potential epigenetic regulation. Instead, histone lysine acetylation and methylation, which are major posttranslational modifications of histone proteins involved in chromatin architecture, are recognized for their crucial roles in regulating the transcription of miRNA genes (Yao et al., 2019). Unlike histone lysine acetylation, which generally causes transcriptional activation, methylation of a histone causes either activation or repression of gene expression, depending on the methylation sites (Barski et al., 2007). Strong correlations have been found between transcriptional repression and methylation at histone H3 lysine 9 (H3K9) and H3K27 (Jaenisch and Bird, 2003; Hyun et al., 2017). To investigate the potential involvement of these histone modifications in CCI-ION, we examined the levels of H3K9 dimethylation (H3K9me2) and H3K27me3. Immunoblot analysis revealed a notable upregulation in both H3K9me2 and H3K27me3 protein levels in the ipsilateral TGs 14 d after CCI-ION compared with the sham groups (Fig. 4*A*; Extended Data Fig. 4-1*B*,*C*; Student's *t* test; for H3K9me2, $p = 0.0045$; for H3K27me3, $p = 0.0001$). ChIP-PCR analysis revealed the amplification of a *miR-216a-3p* promoter fragment from both anti-H3K9me2 and anti-H3K27me3 complexes compared with the relevant IgG controls (Fig. 4*B*; Extended Data Fig. 4-1*D*). ChIP-qPCR measurement revealed that the *miR-216a-3p* gene promoter showed an increased occupancy of H3K27me3 at 14 d after CCI-ION surgery, while the level of H3K9me2 occupancy remained unchanged (Fig. 4*C*; Student's *t* test; for H3K9me2, $p = 0.5246$; for H3K27me3, $p = 0.0174$). Further immunoFISH analysis revealed that H3K27me3 was predominantly located in the nuclei of TG neurons, coexpressing with miR-216a-3p in these neurons (Fig. 4*D*). To investigate the functional involvement of increased H3K27me3 occupancy in nerve injury-induced mechanical allodynia, we administered GSK503 (5 nmol), a potent inhibitor of EZH2 enzymes responsible for catalyzing H3K27me3, directly into the TG. Remarkably, GSK503 treatment significantly reduced the elevated protein expression of H3K27me3 induced by CCI-ION (Fig. 4*E*; Extended Data Fig. 4-1*E*; one-way ANOVA; $p = 0.0058$; CCI-ION vs sham; $p = 0.0039$; CCI-ION + vehicle vs CCI-ION + GSK503). Moreover, ChIP-PCR analysis revealed the amplification of a *miR-216a-3p* promoter fragment from anti-H3K27me3 complexes (Fig. 4*F*; Extended Data Fig. 4-1*F*). In the injured TG after CCI-ION, ChIP-qPCR measurement

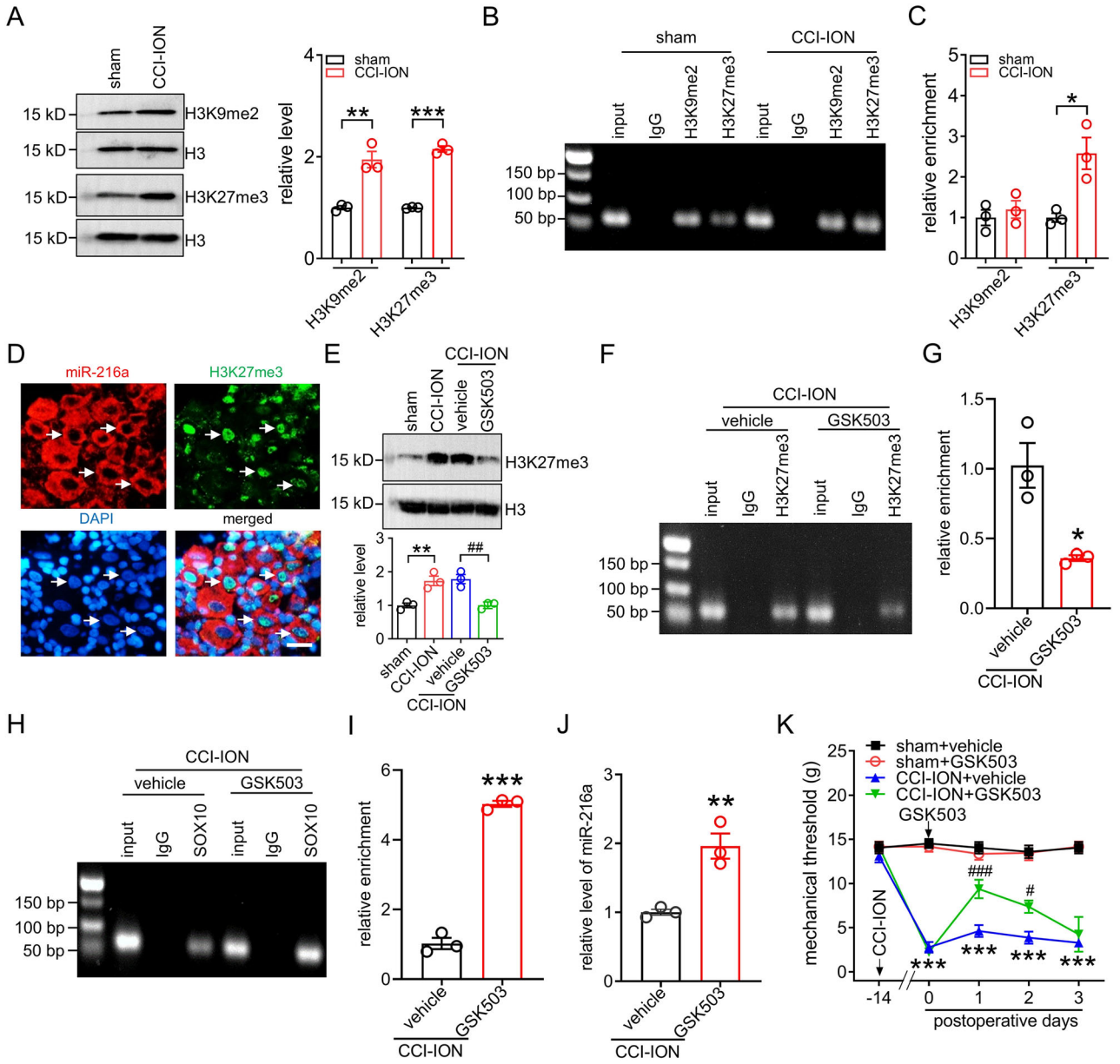

Figure 4. Histone methylation modulates miR-216a-3p expression after nerve injury. ***A***, The protein abundance of H3K9me2 and H3K27me3 in the injured TG at 14 d following CCI-ION operation or sham surgery. The representative blots displayed in the left panel are from three independent experiments. H3 was used as a loading control to normalize the protein abundance. $^{**}p < 0.01$; $^{***}p < 0.001$ (vs sham); by Student's *t* test. $n = 3$ rats/group. Also see Extended Data Figure 4-1, *B* and *C*. ***B***, ***C***, Chromatin immunoprecipitation assays were performed in TGs at 14 d post-CCI-ION or sham surgery using an antibody against H3K9me2 or H3K27me3. The immunoprecipitated DNA was subjected to ChIP-PCR assay (***B***) and quantitative ChIP-qPCR validation (***C***). Data were normalized to their respective input DNA and then compared with the sham groups. $^{*}p < 0.05$ (vs sham), by Student's *t* test. $n = 6$ rats/group. Also see Extended Data Figure 4-1*D*. ***D***, RNA FISH analysis of miR-216a-3p combined with immunostaining of H3K27me3 and DAPI in intact TGs. Colocalizations are indicated by white arrows. Scale bar, 25 µm. ***E***, Effect of GSK503 (5 nmol) on the increased protein abundance of H3K27me3 in the injured TG 14 d after CCI-ION. The blots shown are representative of three independent experiments. $^{**}p < 0.01$ (vs sham); $^{\#\#}p < 0.01$ (vs CCI-ION + vehicle); by one-way ANOVA. $n = 3$ rats/group. Also see Extended Data Figure 4-1*E*. ***F***, ***G***, Chromatin immunoprecipitation assays were performed in the injured TG 14 d post-CCI-ION using an antibody against H3K27me3. The immunoprecipitated DNA was subjected to ChIP-PCR assay (***F***) and quantitative ChIP-qPCR validation (***G***). Data were normalized to the input DNA and then compared with the CCI-ION + vehicle. $^{*}p < 0.05$ (vs CCI-ION + vehicle), by Student's *t* test. $n = 6$ rats/group. Also see Extended Data Figure 4-1*F*. ***H***, ***I***, Chromatin immunoprecipitation assays were performed in the injured TG 14 d post-CCI-ION using an antibody against SOX10. The immunoprecipitated DNA was subjected to ChIP-PCR assay (***H***) and quantitative ChIP-qPCR validation (***I***). Data were normalized to the input DNA and then compared with the CCI-ION + vehicle. $^{***}p < 0.001$ (vs CCI-ION + vehicle), by Student's *t* test. $n = 6$ rats/group. Also see Extended Data Figure 4-1*G*. ***J***, Effect of GSK503 (5 nmol) on the expression level of miR-216a-3p in the injured TG 14 d post-CCI-ION. $^{**}p < 0.01$ (vs CCI-ION + vehicle), by Student's *t* test. $n = 3$ rats/group. ***K***, Effect of GSK503 (5 nmol) on mechanical escape threshold in rats 14 d post-CCI-ION or sham surgery. $^{***}p < 0.001$ (vs sham + vehicle); $^{\#}p < 0.05$; $^{\#\#\#}p < 0.001$ (vs CCI-ION + vehicle); by two-way ANOVA. $n = 7$–8 rats/group.

showed that administration of GSK503 markedly decreased the amplification of a *miR-216a-3p* promoter fragment from anti-H3K27me3 (Fig. 4*G*; Student's *t* test; $p = 0.0148$). Furthermore, ChIP analysis revealed that SOX10 was preferentially enriched at the *miR-216a-3p* promoter in TGs of CCI-ION rats (Fig. 4*H*; Extended Data Fig. 4-1*G*), and this enrichment was significantly increased when the CCI-ION rats were treated with GSK503 (Fig. 4*I*; Student's *t* test; $p = 0.0001$). In addition, intra-TG administration of GSK503 dramatically upregulated the miR-216a-3p expression level in injured TGs

14 d after CCI-ION (Fig. 4*J*; Student's *t* test; $p = 0.0068$). Moreover, administration of GSK503 robustly attenuated the nerve injury-induced mechanical allodynia at 14 d following surgery (Fig. 4*K*; two-way ANOVA; for Days 0, 1, 2, and 3, $p = 0.0001$; CCI-ION + vehicle vs sham + vehicle; for Day 1, $p = 0.0003$; for Day 2, $p = 0.0132$; CCI-ION + GSK503 vs CCI-ION + vehicle). Collectively, these findings demonstrate that nerve injury leads to an upregulation of H3K27me3 modifications, consequently inhibiting the SOX10 binding to the miR-216a-3p promoter and mediating trigeminal neuropathic pain.

miR-216a-3p targets STIM1 in TG neurons

MiRNAs regulate gene expression posttranscriptionally by binding to the 3′-UTR sequences of their target mRNAs (Bartel, 2009). In order to identify potential target genes of miR-216a-3p associated with trigeminal neuropathic pain, we conducted a prediction by using TargetScan (http://www.targetscan.org) and miRwalk (http://mirwalk.umm.uni-heidelberg.de/). Among the candidates, we focused on STIM1 due to its critical role in determining sensory neuronal excitability (Wei et al., 2017), changes of which can directly affect painful conditions such as hyperalgesia and allodynia in vivo (Julius and Basbaum, 2001; Waxman and Zamponi, 2014). To examine whether STIM1 is directly targeted by miR-216a-3p, luciferase reporter constructs carrying the wild-type (STIM1-wt) or the mutant miR-216a-3p targeting sequence (STIM1-mut) within the 3′-UTR of STIM1 were generated (Fig. 5*A*). When cotransfected with miR-216a-3p mimics, the luciferase activity of cells transfected with the STIM1-wt reporter was significantly reduced compared with cells transfected with the negative control, and this reduction was rescued by the STIM1-mut (Fig. 5*B*; Student's *t* test; $p = 0.0076$; miR-216a-wt + miR-216a mimics vs miR-216a-wt + miR-216a NC). The predicted binding sites of miR-216a-3p, as identified by TargetScan, exhibit a high-degree conservation across various vertebrate species (Fig. 5*C*), indicating their functional significance in the regulation of STIM1 expression. ImmunoFISH analysis demonstrated the colocalization of miR-216a-3p with STIM1 in TG neurons (Fig. 5*D*). Statistical analysis showed that ~40.7% of miR-216a-3p-up$^+$ neurons expressed STIM1 and that ~86.5% of STIM1$^+$ neurons expressed miR-216a-3p (Fig. 5*D*). Furthermore, we determined whether manipulation of miR-216a-3p would affect the expression of STIM1. Intra-TG administration of antagomir-216a, but not antagomir-NC, caused a dramatic increase in the protein abundance of STIM1 in intact TGs (Fig. 5*E*; Extended Data Fig. 5-1*A*; one-way ANOVA; $p = 0.0021$; antagmir-216a vs antagmir-NC).

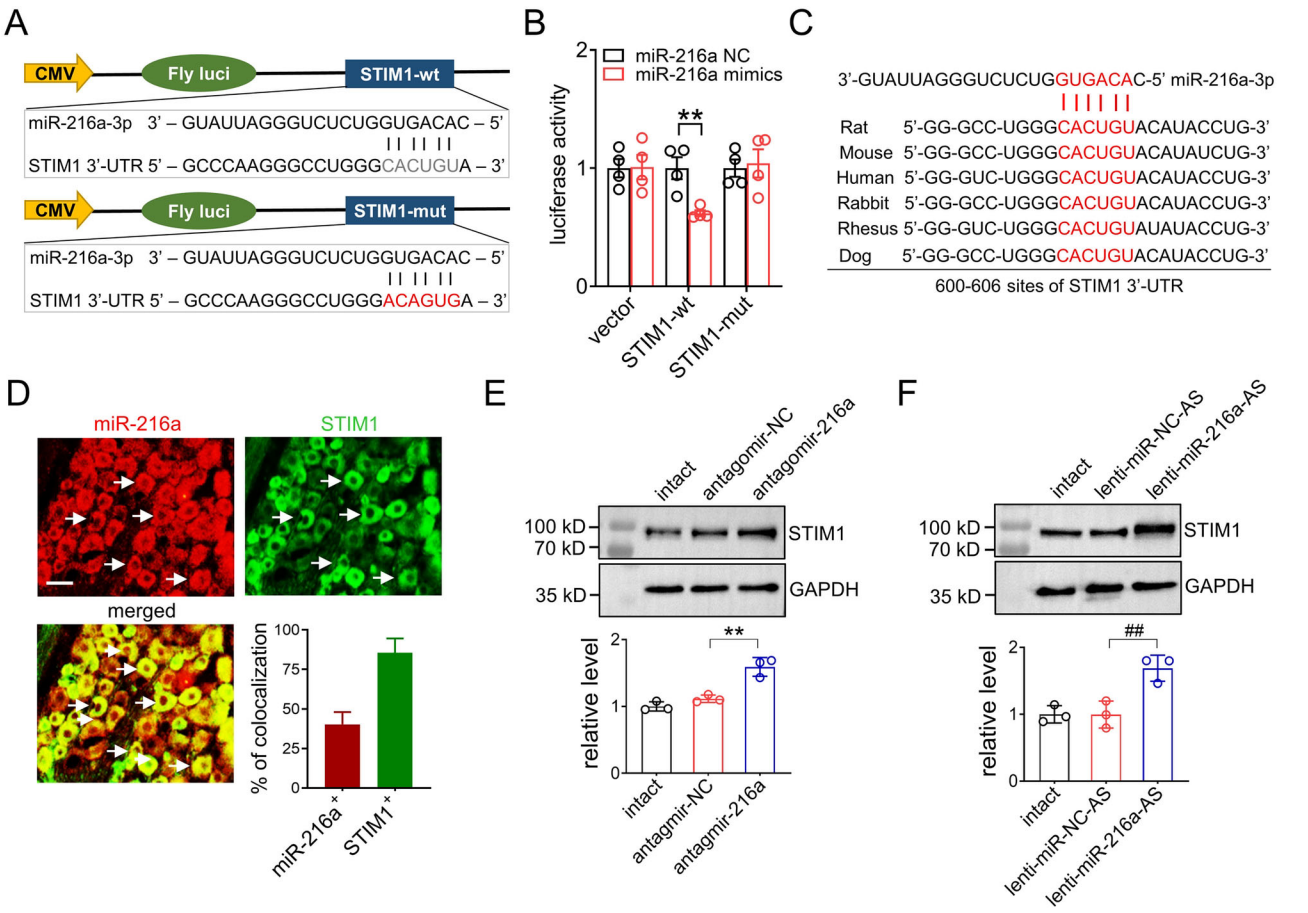

Figure 5. miR-216a-3p targets STIM1. ***A***, Schematic diagrams indicating the luciferase reporter plasmids containing wild-type STIM1 (STIM1-wt) or mutant STIM1 (STIM1-mut). ***B***, Luciferase activities in HEK293T cells after transfection with STIM1-wt/STIM1-mut and miR-216a-3p mimics/negative control (NC). The data shown represent the mean ± SEM of four independent experiments. $^{**}p < 0.01$ (vs miR-216a-3p NC + STIM1-wt), by Student's *t* test. ***C***, Sequences of STIM1 3′-UTRs in various vertebrates. ***D***, RNA FISH analysis of miR-216a-3p combined with immunostaining of STIM1 in the TG of naive rats. Colocalizations are indicated by white arrows. Scale bar, 50 µm. Bar chart demonstrates the percentage of double-labeled neurons among total numbers of miR-216a-3p- or Kv2.1-stained TG neurons. ***E***, ***F***, Effect of antagomir-216a (***E***, $n = 6$ rats/group) or lenti-miR-216a-AS (***F***, $n = 6$ rats/group) on the protein abundance of STIM1 in intact rats. The representative blots displayed in the top panels are from three independent experiments. $^{**}p < 0.01$ (vs antagomir-NC); $^{\#\#}p < 0.01$ (vs lenti-miR-NC-AS); by one-way ANOVA. Also see Extended Data Figure 5-1, *A* and *B*.

In support of these findings, further knockdown of miR-216a-3p by lenti-miR-216a-AS in TG neurons of naive rats significantly upregulated the protein abundance of STIM1 (Fig. 5*F*; Extended Data Fig. 5-1*B*; one-way ANOVA; $p = 0.0075$; lenti-miR-216a-AS vs lenti-miR-NC-AS).

STIM1 participates in regulating TG neuronal excitability

Next, we determined whether STIM1 participated in regulating neuropathic pain behaviors. At 14, 21, and 28 d following CCI-ION, a substantial increase in the protein expression level of STIM1 was observed in the injured TG (Fig. 6*A*; Extended Data Fig. 6-1*A*; one-way ANOVA; for Day 14, $p = 0.0050$; for Day 21, $p = 0.0045$; for Day 28, $p = 0.0041$). In contrast, the sham operation did not result in any significant changes in the basal expression of STIM1 protein in the ipsilateral TG (Fig. 6*B*; Extended Data Fig. 6-1*B*). Furthermore, the abundance of STIM1 protein in the contralateral TG remained unaltered post-CCI-ION (Extended Data Fig. 6-1*C*,*D*). Correlation analysis indicated a significant inverse correlation between the upregulation of STIM1 expression and the downregulation of

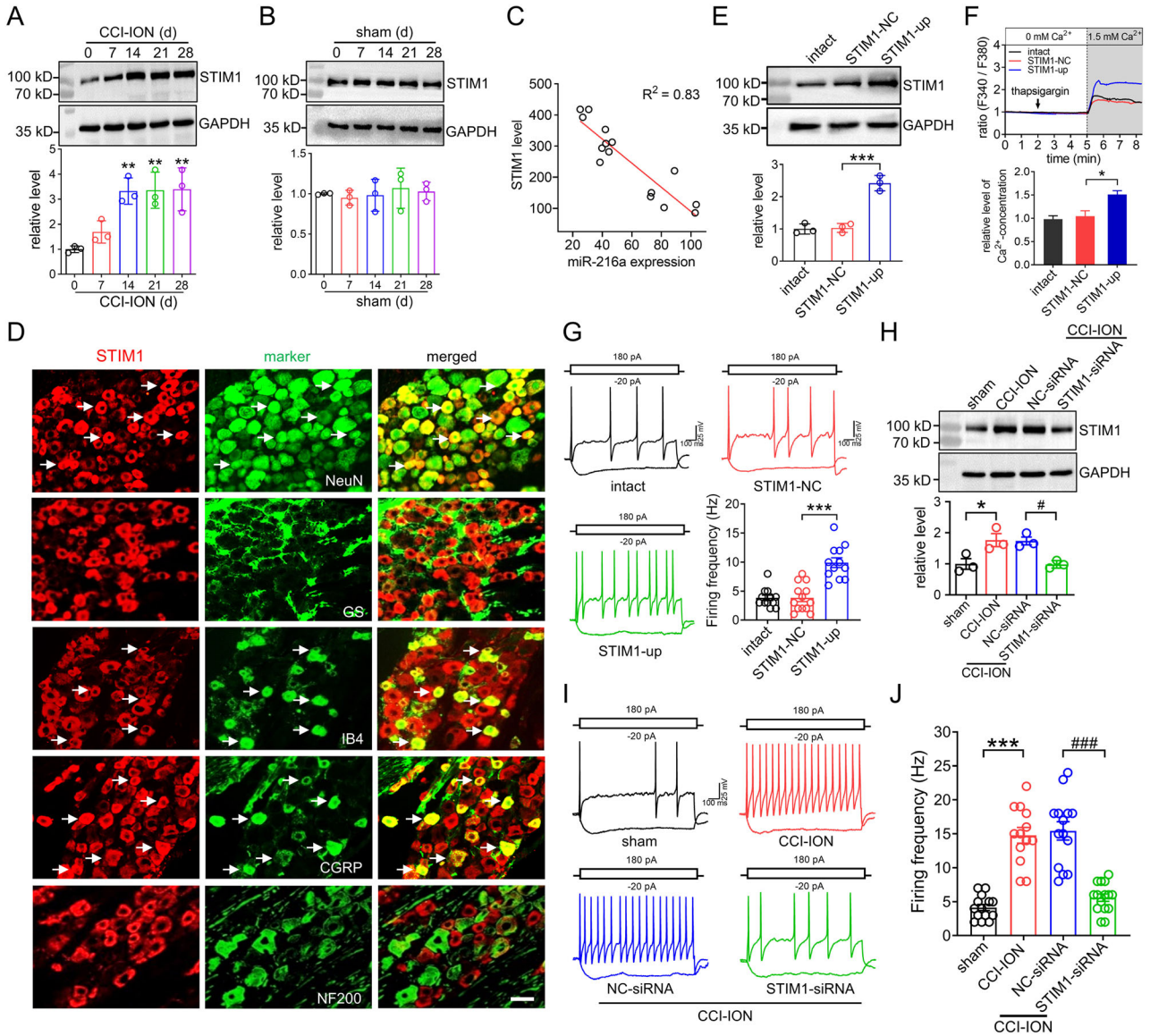

Figure 6. STIM1 participates in regulating neuropathic pain behaviors. ***A***, ***B***, The protein abundance of STIM1 in the injured TG following CCI-ION operation (***A***) or sham surgery (***B***). The blots shown are representative of three independent experiments. $^{**}p < 0.01$ (vs STIM1, Day 0), by one-way ANOVA. $n = 6$ rats/group. Also see Extended Data Figure 6-1, *A* and *B*. ***C***, The expression level of miR-216a-3p showed an inverse correlation with the STIM1 mRNA level in the TG of rats at Days 0, 7, 14, 21, and 28 post-CCI-ION operation ($R^2 = 0.83$). ***D***, Double immunostaining of STIM1 (red) with NeuN, GS, IB_4, CGPR, and NF200 (green) in intact TGs. Colocalizations are indicated by white arrows. Scale bar, 50 µm. ***E***, Protein abundance of STIM1 in the TGs of the STIM1-up–treated groups. $^{***}p < 0.001$ (vs STIM1-NC), by one-way ANOVA. Representative blots from three independent experiments are shown. $n = 6$ rats/group. Also see Extended Data Figure 6-1*E*. ***F***, Fluorescence analysis of Ca^{2+} influx in rat TG neurons treated with either STIM1-up or STIM1-NC. The top panel displayed representative traces from rats in the intact, STIM1-NC and STIM1-up groups. Ca^{2+} store depletion was induced by removing Ca^{2+} and adding 2 µM thapsigargin. The bottom panel presented summary data illustrating the intracellular Ca^{2+} levels from three independent experiments. $^{*}p < 0.05$ (vs STIM1-NC), one-way ANOVA. $n = 200$–250 neurons/group from three rats. ***G***, Representative traces and summary of results showing that intra-TG application of STIM1-up increased the action potential firing rate. $n = 12$–13 neurons/group. $^{***}p < 0.001$ (vs STIM1-NC), by one-way ANOVA. ***H***, Effect of chemically modified STIM1-siRNA on the protein expression of STIM1 in CCI-ION rats. The representative blots displayed in the top panels are from three independent experiments. $^{*}p < 0.05$ (vs sham); $^{\#}p < 0.05$ (vs CCI-ION + NC-siRNA); by one-way ANOVA. $n = 6$ rats/group. Also see Extended Data Figure 6-1*F*. ***I***, ***J***, Representative traces (***I***) and bar graph (***J***) showing that intra-TG application of STIM1-siRNA prevented the CCI-ION–induced increase in the action potential firing rate. $n = 13$–15 neurons/group. $^{***}p < 0.001$ (vs sham); $^{\#\#\#}p < 0.001$ (vs CCI-ION + NC-siRNA); by one-way ANOVA.

miR-216a-3p (Fig. 6C). Immunostaining of TG sections indicated that STIM1 coexisted with NeuN but was not detected in GS-labeled cells, indicating that STIM1 is expressed predominantly in TG neurons (Fig. 6D). Further double-staining analysis revealed that STIM1 primarily coexpressed with CGRP and IB_4, suggesting nociceptive neurons but showed comparatively less colocalization with cells expressing 200 kD neurofilament protein (NF200) (Fig. 6D). Next, we investigated whether STIM1 participated in regulating TG neuronal excitability. Local induction of STIM1 in intact TG neurons through intra-TG administration of STIM1-up significantly increased STIM1 protein levels (Fig. 6E; Extended Data Fig. 6-1E; one-way ANOVA; $p = 0.0002$; STIM1-up vs STIM1-NC) and resulted in a higher intracellular calcium level compared with TG neurons treated with STIM1-NC, following passive store depletion induced by thapsigargin (Fig. 6F; one-way ANOVA; $p = 0.0277$; STIM1-up vs STIM1-NC). Additionally, STIM1-up administration, but not STIM1-NC, markedly induced TG neuronal hyperexcitability (Fig. 6G; one-way ANOVA; $p = 0.0001$; STIM1-up vs STIM1-NC). Intra-TG injection of chemically modified STIM1-siRNA reduced the nerve injury-induced increase in STIM1 protein levels (Fig. 6H; Extended Data Fig. 6-1F; one-way ANOVA; $p = 0.0297$; CCI-ION vs sham; $p = 0.0319$; CCI-ION + NC-siRNA vs CCI-ION + STIM1-siRNA). Further current-clamp recordings revealed that DiI-labeled small TG neurons from CCI-ION rats exhibited a higher firing frequency of action potentials (Fig. 6I,J) compared with those from sham-operated rats. Notably, application of STIM1-siRNA, but not the NC-siRNA, abolished CCI-ION–induced neuronal hyperexcitability (Fig. 6I,J; one-way ANOVA; $p = 0.0001$; CCI-ION vs sham; $p = 0.0001$; CCI-ION + STIM1-siRNA vs CCI-ION + NC-siRNA).

STIM1 participates in miR-216a-3p–mediated neuropathic analgesia

We further investigated whether STIM1 contributes to chronic neuropathic pain by injecting chemically modified STIM1-siRNA (or the corresponding negative control NC-siRNA) into the unilateral TG 14 d after CCI-ION. Our results showed that STIM1-siRNA administration, but not NC-siRNA, significantly reduced mechanical allodynia (Fig. 7A; two-way ANOVA; for Days 0, 1, 3, 5, and 7, $p = 0.0001$; CCI-ION + NC-siRNA vs sham + NC-siRNA; for Days 3, 5, and 7, $p = 0.0001$; CCI-ION + STIM1-siRNA vs CCI-ION + NC-siRNA) and heat hyperalgesia (Fig. 7B; two-way ANOVA; for Day 0, $p = 0.0018$; for Day 1, $p = 0.0034$; for Day 3, $p = 0.0027$; for Day 5, $p = 0.0023$; for

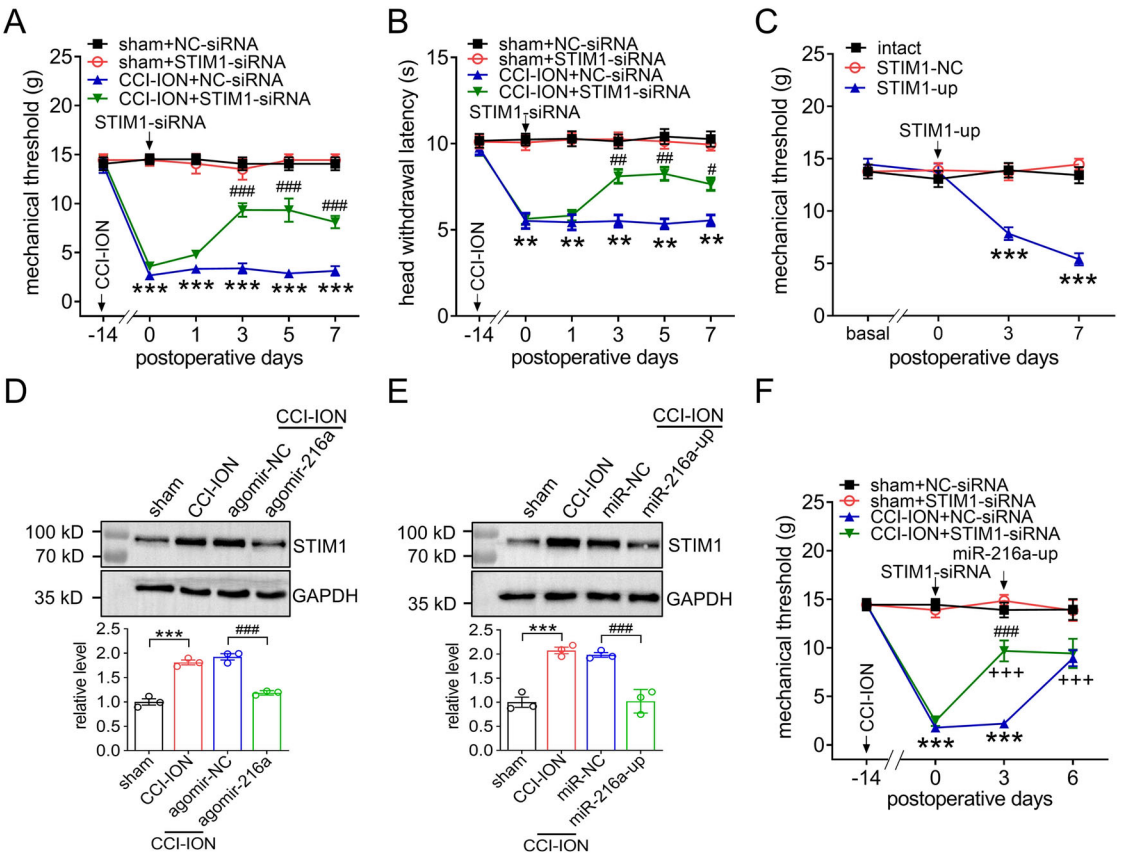

Figure 7. miR-216a-3p regulates nociceptive behaviors via STIM1. ***A***, ***B***, Effect of STIM1-siRNA on nerve injury-induced mechanical allodynia (***A***) and heat hyperalgesia (***B***). $^{**}p < 0.01$; $^{***}p < 0.001$ (vs sham + NC-siRNA); $^{\#}p < 0.05$; $^{\#\#}p < 0.01$; $^{\#\#\#}p < 0.001$ (vs CCI-ION + NC-siRNA); by two-way ANOVA. $n = 7$–8 rats/group. ***C***, Intra-TG injection of STIM1-up in naive rats resulted in mechanical hypersensitivity. $^{***}p < 0.001$ (vs STIM1-NC), by two-way ANOVA. $n = 5$–6 rats/group. ***D***, Immunoblot analysis revealing that intra-TG administration of agomir-216a (but not agomir-NC) reversed the nerve injury-induced increase in the protein abundance of STIM1. The representative blots displayed in the top panels are from three independent experiments. $^{***}p < 0.001$ (vs sham); $^{\#\#\#}p < 0.001$ (vs CCI-ION + agomir-NC); by one-way ANOVA. $n = 3$ rats/group. Also see Extended Data Figure 7-1A. ***E***, Intra-TG injection of lenti-miR-216a-up suppressed the nerve injury-induced increase in the protein abundance of STIM1. $^{***}p < 0.001$ (vs sham); $^{\#\#\#}p < 0.001$ (vs CCI-ION + miR-NC); by one-way ANOVA. $n = 3$ rats/group. The blots shown are representative of three independent experiments. Also see Extended Data Figure 7-1B. ***F***, Effect of STIM1-siRNA (Day 0) versus NC-siRNA on miR-216a-up (Day 3)-induced attenuation of mechanical allodynia in CCI-ION rats. $^{***}p < 0.001$ (vs sham + NC-siRNA); $^{\#\#\#}p < 0.001$ (vs CCI-ION + NC-siRNA, Day 3); $^{+++}p < 0.001$ (vs CCI-ION + STIM1-siRNA, Day 0); by two-way ANOVA. $n = 7$–8 rats/group.

Day 7, $p = 0.0026$; CCI-ION + NC-siRNA vs sham + NC-siRNA; for Day 3, $p = 0.0074$; for Day 5, $p = 0.0028$; for Day 7, $p = 0.0161$; CCI-ION + STIM1-siRNA vs CCI-ION + NC-siRNA) from Day 3 to Day 7 following the injection. Additionally, in naive rats, unilateral intra-TG injection of STIM1-up significantly induced mechanical hypersensitivity on Day 3, which lasted for at least 7 d, while NC-up treatment did not produce such effects (Fig. 7*C*; two-way ANOVA; for Days 3 and 7, $p = 0.0001$; STIM1-up vs STIM1-NC). Next, we examined whether STIM1 is involved in miR-216a-3p–mediated neuropathic analgesia. We first examined whether the regulation of miR-216a-3p alters STIM1 protein expression in the injured TG. First, we unilaterally injected agomir-216a or agomir-NC into the TG of CCI-ION rats. Intra-TG injection of agomir-216a reversed the increased protein abundance in STIM1 14 d after CCI-ION (Fig. 7*D*; Extended Data Fig. 7-1*A*; one-way ANOVA; $p = 0.0001$; CCI-ION vs sham; $p = 0.0001$; CCI-ION + agomir-216a vs CCI-ION + agomir-NC). To further corroborate these findings, we locally overexpressed miR-216a-3p in TG neurons by intra-TG administration of miR-216a-up. Immunoblot analysis showed that administration of miR-216a-up suppressed the increased protein abundance of STIM1 induced by CCI-ION (Fig. 7*E*; Extended Data Fig. 7-1*B*; one-way ANOVA; $p = 0.0002$; CCI-ION vs sham; $p = 0.0005$; CCI-ION + miR-216a-up vs CCI-ION + miR-NC). In order to better understand the involvement of STIM1 in miR-216a-3p–induced nociceptive behaviors, we conducted local administration of STIM1-siRNA in conjunction with miR-216a-up in the injured TG of rats with CCI-ION. On Day 0, STIM1-siRNA was injected into the TG, followed by the administration of miR-216a-up on Day 3. In comparison with NC-siRNA groups (negative control), the STIM1-siRNA treatment robustly attenuated the mechanical allodynia induced by CCI-ION (Fig. 7*F*; two-way ANOVA; for Days 0 and 3, $p = 0.0001$; for Day 3, $p = 0.0001$; CCI-ION + STIM1-siRNA vs CCI-ION + NC-siRNA; for Days 3 and 6, $p = 0.0001$; CCI-ION + STIM1-siRNA, Days 3 and 6, vs STIM1-siRNA, Day 0). Interestingly, additional administration of miR-216a-up on Day 3 did not exhibit any additional effect on the mechanical threshold in CCI-ION rats treated with STIM1-siRNA. This was demonstrated by the consistent stability of the mechanical threshold from Day 3 to Day 6 following miR-216a-up application (Fig. 7*F*). Contrastingly, in the NC-siRNA–treated CCI-ION rats, injection of miR-216a-up significantly increased the mechanical pain threshold (Fig. 7*F*). Together, these findings emphasized the participation of STIM1 in neuropathic pain behaviors induced by miR-216a-3p downregulation in TG neurons.

Discussion

In the present study, we identified a new epigenetic regulatory mechanism driven by miR-216a-3p in sensory neurons that contributes to trigeminal-mediated neuropathic pain. Local induction of miR-216a-3p in the injured TG, either pharmacologically or genetically, effectively alleviates mechanical allodynia and heat hyperalgesia. The underlying mechanism involves the H3K27-mediated histone trimethylation, which suppresses the TF SOX10 binding to the *miR-216a-3p* promoter. This leads to a decrease in miR-216a-3p expression and subsequently promotes the development of neuropathic pain through regulating STIM1 (as shown in Fig. 8). Manipulating miR-216a-3p and its relevant epigenetic factors could potentially serve as novel therapeutic targets for the treatment of neuropathic pain.

MiRNAs play a crucial role in regulating gene expression by binding to the 3′-UTRs of their target mRNAs posttranscriptionally (Bartel, 2009). Recent research indicates that there are specific alterations in miRNA expression within different tissues during various pain conditions, such as inflammatory pain, neuropathic pain, and cancer-related pain (Favereaux et al., 2011;

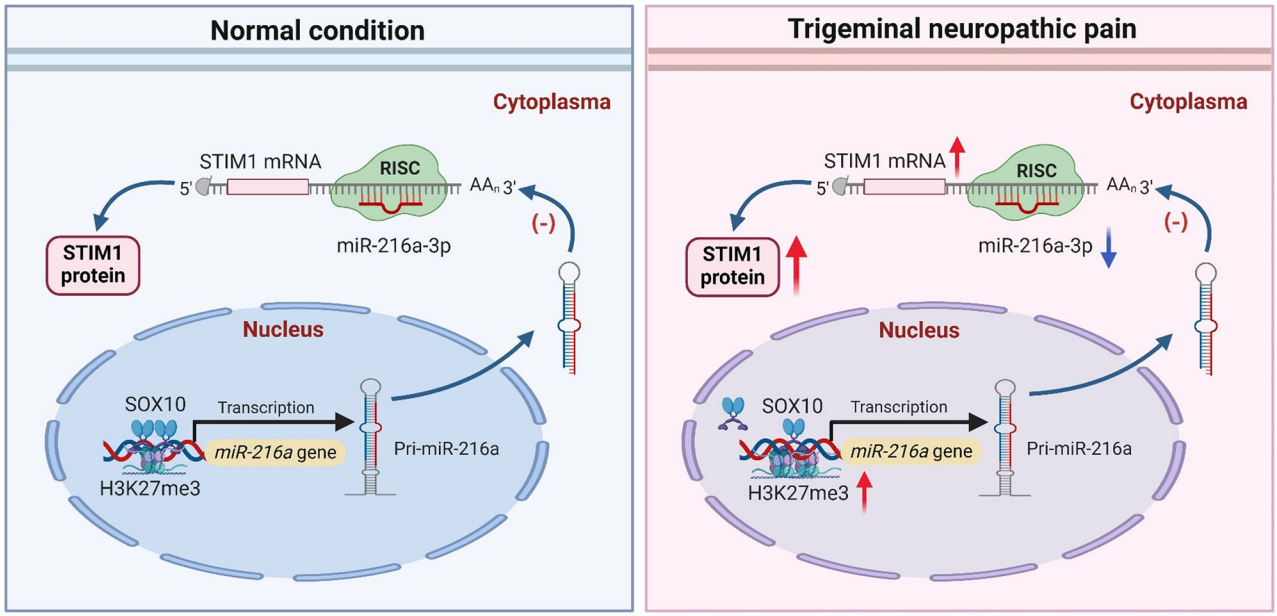

Figure 8. Schematic diagrams demonstrating the sensory H3K27me3-dependent SOX10/miR-216a-3p/STIM1 signaling axis in neuropathic pain. Left panel, A hypomethylated miR-216a-3p promoter region under normal conditions, resulting in a normal miR-216a-3p level in TG neurons. Right panel, H3K27me3-mediated downregulation of miR-216a-3p in sensory neurons regulates trigeminal-mediated neuropathic pain behaviors via targeting STIM1. First, peripheral nerve injury promotes the trimethylation of H3 at lysine 27, thereby suppressing the TF SOX10 binding to the *miR-216a-3p* promoter and resulting in the downregulation of miR-216a-3p expression. Next, mature single-stranded miR-216a-3p, guided by the RNA-induced silencing complex, recognizes and binds the complementary sequence on the STIM1 mRNA within the 3′-UTR. This binding triggers the degradation of the target mRNA. Finally, the downregulation of miR-216a-3p as a result of nerve injury leads to an increase in STIM1 protein expression, which subsequently results in chronic neuropathic pain symptoms.

Pan et al., 2016). Studies have shown that manipulating the expression of specific miRNAs can prevent and reverse these nociceptive behaviors (Favereaux et al., 2011; Pan et al., 2016). However, the mechanisms underlying the modulation of miRNA expression during pathophysiological processes are not yet well understood. Further research is needed to uncover the regulatory mechanisms that govern miRNA expression changes in pain-related pathologies. Modification of histone and DNA methylation are the two major epiregulatory mechanisms that have profound effects on controlling gene expression (Guan et al., 2009; Riccio, 2010). Previous studies have indicated that DNA methylation and hydroxylation regulate miRNA expression in the context of inflammatory pain (Pan et al., 2014, 2016). Upon examining the gene sequence of miR-216a-3p, it was determined that there were no CpG islands present in its promoter region. However, it was observed that peripheral nerve injury led to a notable upregulation in the expression level of H3K27me3 in the miR-216a-3p promoter, while the H3K9me2 level remained unchanged. These modifications were found to be involved in regulating trigeminal-mediated neuropathic pain. The H3K27me3-mediated histone methylation of the miR-216a-3p promoter region resulted in the suppression of SOX10 binding to miR-216a-3p, leading to a decrease in its expression. Our findings are consistent with previous studies that demonstrated increased levels of H3K9me2 and H3K27me3 in the rat dorsal root ganglion (DRG) following spinal nerve ligation (SNL; Ghosh et al., 2022). Interestingly, data from the same animal model also revealed that H3K9me2, but not H3K27me3, decreased the expression levels of K^+ channels and played a critical role in pain regulation (Laumet et al., 2015). However, other studies have also shown that both occupancies of two repressive histone marks (H3K9me2 and H3K27me3) around the promoter region of Panx1 as well as Cnr2 in the DRG were decreased using the same SNL model (Zhang et al., 2015). Although further investigation is necessary to fully understand the specific mechanisms underlying histone modifications and their effects on gene expression in different tissue and cell types, it is likely that the presence of different histone dimethyltransferases or demethylases, as well as the use of different neuropathic pain models and gene promoters, could contribute to the observed discrepancies in histone modifications. Variability in these factors may influence the extent and nature of histone modifications, leading to differences in gene regulation and ultimately contributing to the variability in pain responses observed in different experimental settings. Therefore, it is important to carefully consider these factors when interpreting and comparing findings from different studies investigating histone modifications in the context of neuropathic pain. For instance, the increased H3K27me3 occupancy at gene promoters mediated by the EZH2 methyltransferase generally mediates transcriptional repression (Barski et al., 2007), while the regulation of H3K9me2 is mediated by G9a proteins (Schuettengruber et al., 2007). Moreover, evidence has suggested the balance between methylation and acetylation of H3K9 or H3K27 influencing gene regulation (Gupta-Agarwal et al., 2012). Unlike acetylation of histone, which generally causes transcriptional activation, methylation of a histone causes either activation or repression of gene expression, depending on the methylation sites (Kurdistani and Grunstein, 2003). For instance, acetylation at K9, K14, K18, and K27 of H3 results in transcriptional activation, while deacetylation of these positions correlates with repression (Berger, 2007). While it is worth considering the possibility of concurrent alterations in histone modification, such as a decrease in H3K18me1 and an increase in H3K18ac occupancy, following nerve injury, which could potentially impact the binding of SOX10 to the *miR-216a-3p* promoter, this particular aspect is beyond the scope of the current study.

In this study, in situ hybridization revealed widespread miR-216a-3p expression in both small-sized TG neurons, putative nociceptive neurons, and medium-sized TG neurons. The distribution of miR-216a-3p expression appears to coincide with that of STIM1, as STIM1 protein expression is also detected in small- to medium-sized TG neurons. In addition, we found that functional blockade of miR-216a-3p can increase STIM1 protein expression, suggesting that TG neurons express both miR-216a-3p and STIM1. In rat TG neurons, immunoreactivity for STIM1 was mainly labeled with IB_4 and CGRP, markers of nonpeptidergic and peptidergic nociceptive neurons, while few STIM1-labeled TG neurons coexpressed NF200. This expression pattern was consistent with previous data showing mainly location of STIM1 in small- to medium-sized sensory neurons of dorsal root ganglia (DRG; Wei et al., 2017), while some studies have shown no preferential expression of STIM1 in DRG subpopulations of different neuronal sizes (Gemes et al., 2011). Interestingly, in the same study, it has been demonstrated that STIM1 is also present in the cytoplasm of DRG satellite glial cells; however, these findings seem to be contradictory to those of most related studies. Indeed, STIM1 was specifically and significantly expressed in neurons but not astrocytes and microglia in the spinal dorsal horn (Wang et al., 2023), while some studies have demonstrated that the SOCC family including STIM1 is expressed in spinal astrocytes (Gao et al., 2016). Though this discrepancy requires further investigation, the expression profile of STIM1 might vary across tissue types or animal species. Additionally, it is important to acknowledge that while peripheral tissue nociceptors, such as the TG and DRG, exhibit functional similarities, they also display distinct developmental lineages. Recent genomic studies have revealed that these nociceptors possess unique gene expression profiles (Kogelman et al., 2017; Megat et al., 2019; Korczeniewska et al., 2020). Furthermore, the expression levels of STIM proteins can vary during different developmental stages in certain tissues. For instance, while STIM1 is present in neonatal cardiomyocytes, it is absent in adult cardiomyocytes (Luo et al., 2012).

Nonetheless, the role of the STIM1 in trigeminal-mediated nociceptive processing is still unknown. STIM1, the pivotal component of store-operated calcium channels (Stathopulos et al., 2006), plays critical roles in regulating cytoplasmic Ca^{2+} homeostasis and neuronal excitability and is associated with neurological disorders including stroke, Parkinson's disease, and pain processing (Gao et al., 2016; Kuang et al., 2016; Qi et al., 2016; Wei et al., 2017). In our present study, local induction of STIM1 effectively raised the intracellular calcium level and increased TG neuronal excitability in naive rats. Consistent with our findings, previous studies have also shown that STIM1 overexpression is sufficient to increase SOCE current both in cardiomyocytes (Hulot et al., 2011) and gastrointestinal stromal tumors cells (Yang et al., 2018), even though SOCE requires both STIM and Orai proteins in a heterologous expression system using HEK293 cells (Hoover and Lewis, 2011). Similarly, Limnander et al. (2011) have also observed that higher amounts of STIM1 protein may contribute to amplify SOCE. Nevertheless, the relationship between increased SOCE and neuronal excitability remains controversial. For instance, Wei et al. (2017) suggest that SOCE has an excitatory effect in DRG neurons, whereas Gemes et al. (2011) provided solid evidence that

increased SOCE following nerve injury is a compensatory mechanism to reduce neuronal excitability. Although these discrepancies have yet to be clarified and needs further investigation, current-clamp recordings in our present study revealed that intra-TG injection of chemically modified STIM1-siRNA, but not NC-siRNA, abolished CCI-ION–induced neuronal hyperexcitability. In contrast, local overexpression of STIM1 in TG neurons via intra-TG administration of STIM1-up markedly increased TG neuronal excitability. Our results also show that the upregulated expression of the STIM1 is triggered by peripheral nerve injury and that knockdown of STIM1 expression in TG neurons alleviates CCI-ION–induced mechanical allodynia and heat hyperalgesia. Consistent with our current findings, knocking down STIM1 in the DRG or blockage of Orai channels with pharmacological tools decreased neuronal excitability and attenuates chronic pain (Wei et al., 2017). Moreover, it has been suggested that increased STIM1 protein expression in the spinal dorsal horn results in remifentanil-induced postoperative hyperalgesia (Zhou et al., 2021). In the current study, miR-216a-3p governs STIM1 expression through recognition of the 3′-UTR sequence of STIM1 mRNAs. Our study demonstrated that overexpressing miR-216a-3p in injured TG neurons did not exhibit any additive effects on the mechanical threshold in STIM1-treated CCI-ION rats. While our study demonstrated the significance of miR-216a-3p targeting of STIM1 in regulating neuropathic pain, it is important to acknowledge that STIM1 may not be the sole factor participating in miR-216a-3p–mediated nociceptive behaviors, since our RNA-seq data indicated that the expression of a number of miR-216a-3p target genes was upregulated, such as *SLC10A4*, *SNAPC2*, *HPRT1*, and *SZRD1* (GEO accession number GSE192803), and they may contribute to the alteration of the nociceptive response as well. In addition, previous research revealed that miR-216a-3p might regulate the expression of a variety of genes. For example, miR-216a-3p inhibits osteogenic differentiation of human adipose-derived stem cells by targeting Wnt3a (Liang et al., 2022) and promotes sorafenib sensitivity in hepatocellular carcinoma by affecting MAPK14 expression and activity (Wan et al., 2020). Moreover, miR-216a-3p participates in the pathogenesis of Parkinson's disease via regulating the expression of Bcl-2-associated X protein (Wei et al., 2017). Therefore, it is crucial to recognize that while we have elucidated the participation of miR-216a-3p in regulating neuropathic pain through its targeting of STIM1, there may be other mechanisms by which miR-216a-3p contributes to pain processing. It is essential to continue studying these potential mechanisms in future research. A comprehensive understanding of the regulatory mechanisms of miR-216a-3p in sensory neurons will not only enhance our knowledge of neuropathic pain pathophysiology but also shed light on its broader roles in various physiological and pathological processes.

In summary, our study reveals a novel H3K27me3-dependent SOX10/miR-216a-3p/STIM1 signaling pathway in sensory neurons, which plays a role in the development of trigeminal-mediated neuropathic pain. We found that nerve injuries lead to an increase in H3K27me3, which inhibits the SOX10 binding to the miR-216a-3p promoter and subsequently reduces the expression level of miR-216a-3p. This downregulation of miR-216a-3p contributes to the development and maintenance of neuropathic pain by regulating STIM1 expression. The discovery of epigenetic regulators like SOX10 and miR-216a-3p in controlling STIM1 in peripheral sensory neurons opens up new possibilities for developing innovative therapeutic strategies and drug targets for chronic neuropathic pain.

Data Availability

The miRNA-seq data for this study can be accessed through the National Center for Biotechnology Information GEO database using the accession numbers GSE192803. All study data are included in the article and supporting information.

References

Baron R, Binder A, Wasner G (2010) Neuropathic pain: diagnosis, pathophysiological mechanisms, and treatment. Lancet Neurol 9:807–819.

Barski A, Cuddapah S, Cui K, Roh TY, Schones DE, Wang Z, Wei G, Chepelev I, Zhao K (2007) High-resolution profiling of histone methylations in the human genome. Cell 129:823–837.

Bartel DP (2009) MicroRNAs: target recognition and regulatory functions. Cell 136:215–233.

Berger SL (2007) The complex language of chromatin regulation during transcription. Nature 447:407–412.

Cao J, Zhang Y, Wu L, Shan L, Sun Y, Jiang X, Tao J (2019) Electrical stimulation of the superior sagittal sinus suppresses A-type K(+) currents and increases P/Q– and T-type Ca(2+) currents in rat trigeminal ganglion neurons. J Headache Pain 20:87.

Favereaux A, et al. (2011) Bidirectional integrative regulation of Cav1.2 calcium channel by microRNA miR-103: role in pain. EMBO J 30:3830–3841.

Finnerup NB, Kuner R, Jensen TS (2021) Neuropathic pain: from mechanisms to treatment. Physiol Rev 101:259–301.

Gao X, Xia J, Munoz FM, Manners MT, Pan R, Meucci O, Dai Y, Hu H (2016) STIMs and Orai1 regulate cytokine production in spinal astrocytes. J Neuroinflammation 13:126.

Gemes G, Bangaru ML, Wu HE, Tang Q, Weihrauch D, Koopmeiners AS, Cruikshank JM, Kwok WM, Hogan QH (2011) Store-operated Ca^{2+} entry in sensory neurons: functional role and the effect of painful nerve injury. J Neurosci 31:3536–3549.

Ghosh K, Zhang GF, Chen H, Chen SR, Pan HL (2022) Cannabinoid CB2 receptors are upregulated via bivalent histone modifications and control primary afferent input to the spinal cord in neuropathic pain. J Biol Chem 298:101999.

Guan JS, et al. (2009) HDAC2 negatively regulates memory formation and synaptic plasticity. Nature 459:55–60.

Gupta-Agarwal S, Franklin AV, Deramus T, Wheelock M, Davis RL, McMahon LL, Lubin FD (2012) G9a/GLP histone lysine dimethyltransferase complex activity in the hippocampus and the entorhinal cortex is required for gene activation and silencing during memory consolidation. J Neurosci 32:5440–5453.

Hamm CA, Costa FF (2015) Epigenomes as therapeutic targets. Pharmacol Ther 151:72–86.

Hoover PJ, Lewis RS (2011) Stoichiometric requirements for trapping and gating of Ca2+ release-activated Ca2+ (CRAC) channels by stromal interaction molecule 1 (STIM1). Proc Natl Acad Sci U S A 108:13299–13304.

Huang Z, Zhang Y, Wang S, Qi R, Tao Y, Sun Y, Jiang D, Jiang X, Tao J (2024) FOXD3-mediated transactivation of ALKBH5 promotes neuropathic pain via m(6)A-dependent stabilization of 5-HT3A mRNA in sensory neurons. Proc Natl Acad Sci U S A 121:e2312861121.

Hulot JS, et al. (2011) Critical role for stromal interaction molecule 1 in cardiac hypertrophy. Circulation 124:796–805.

Hyun K, Jeon J, Park K, Kim J (2017) Writing, erasing and reading histone lysine methylations. Exp Mol Med 49:e324.

Jaenisch R, Bird A (2003) Epigenetic regulation of gene expression: how the genome integrates intrinsic and environmental signals. Nat Genet 33: 245–254.

John B, Enright AJ, Aravin A, Tuschl T, Sander C, Marks DS (2004) Human microRNA targets. PLoS Biol 2:e363.

Julius D, Basbaum AI (2001) Molecular mechanisms of nociception. Nature 413:203–210.

Kc E, Islam J, Park YS (2022) Trigeminal ganglion itself can be a viable target to manage trigeminal neuralgia. J Headache Pain 23:150.

Kogelman LJA, Christensen RE, Pedersen SH, Bertalan M, Hansen TF, Jansen-Olesen I, Olesen J (2017) Whole transcriptome expression of trigeminal ganglia compared to dorsal root ganglia in *Rattus norvegicus*. Neuroscience 350:169–179.

Kopruszinski CM, Reis RC, Bressan E, Reeh PW, Chichorro JG (2015) Vitamin B complex attenuated heat hyperalgesia following infraorbital

nerve constriction in rats and reduced capsaicin in vivo and in vitro effects. Eur J Pharmacol 762:326–332.
Korczeniewska OA, et al. (2020) Differential gene expression changes in the dorsal root versus trigeminal ganglia following peripheral nerve injury in rats. Eur J Pain 24:967–982.
Kuang XL, Liu Y, Chang Y, Zhou J, Zhang H, Li Y, Qu J, Wu S (2016) Inhibition of store-operated calcium entry by sub-lethal levels of proteasome inhibition is associated with STIM1/STIM2 degradation. Cell Calcium 59:172–180.
Kurdistani SK, Grunstein M (2003) Histone acetylation and deacetylation in yeast. Nat Rev Mol Cell Biol 4:276–284.
Laumet G, et al. (2015) G9a is essential for epigenetic silencing of K(+) channel genes in acute-to-chronic pain transition. Nat Neurosci 18:1746–1755.
Liang D, Song G, Zhang Z (2022) miR-216a-3p inhibits osteogenic differentiation of human adipose-derived stem cells via Wnt3a in the Wnt/beta-catenin signaling pathway. Exp Ther Med 23:309.
Limnander A, Depeille P, Freedman TS, Liou J, Leitges M, Kurosaki T, Roose JP, Weiss A (2011) STIM1, PKC-δ and RasGRP set a threshold for proapoptotic Erk signaling during B cell development. Nat Immunol 12:425–433.
Liu H, Yu K, Ma P, Xiong L, Wang M, Wang W (2019) Long noncoding RNA myocardial infarction-associated transcript regulated the pancreatic stellate cell activation to promote the fibrosis process of chronic pancreatitis. J Cell Biochem 120:9547–9555.
Luo X, Hojayev B, Jiang N, Wang ZV, Tandan S, Rakalin A, Rothermel BA, Gillette TG, Hill JA (2012) STIM1-dependent store-operated Ca(2)(+) entry is required for pathological cardiac hypertrophy. J Mol Cell Cardiol 52:136–147.
Martin YB, Avendano C (2009) Effects of removal of dietary polyunsaturated fatty acids on plasma extravasation and mechanical allodynia in a trigeminal neuropathic pain model. Mol Pain 5:8.
Megat S, et al. (2019) Differences between dorsal root and trigeminal ganglion nociceptors in mice revealed by translational profiling. J Neurosci 39: 6829–6847.
Messlinger K, Russo AF (2019) Current understanding of trigeminal ganglion structure and function in headache. Cephalalgia 39:1661–1674.
Ni R, Liu H, Song G, Fu X, Deng B, Xu Z, Dai S, Huang G (2023) MiR-216a-3p inhibits the proliferation and invasion of fibroblast-like synoviocytes by targeting dual-specificity phosphatase 5. Int J Rheum Dis 26:699–709.
Pan Z, et al. (2014) Epigenetic modification of spinal miR-219 expression regulates chronic inflammation pain by targeting CaMKIIgamma. J Neurosci 34:9476–9483.
Pan Z, Zhang M, Ma T, Xue ZY, Li GF, Hao LY, Zhu LJ, Li YQ, Ding HL, Cao JL (2016) Hydroxymethylation of microRNA-365-3p regulates nociceptive behaviors via Kcnh2. J Neurosci 36:2769–2781.
Qi R, Cao J, Sun Y, Li Y, Huang Z, Jiang D, Jiang XH, Snutch TP, Zhang Y, Tao J (2022) Histone methylation-mediated microRNA-32-5p downregulation in sensory neurons regulates pain behaviors via targeting Cav3.2 channels. Proc Natl Acad Sci U S A 119:e2117209119.
Qi Z, Wang Y, Zhou H, Liang N, Yang L, Liu L, Zhang W (2016) The central analgesic mechanism of YM-58483 in attenuating neuropathic pain in rats. Cell Mol Neurobiol 36:1035–1043.
Riccio A (2010) Dynamic epigenetic regulation in neurons: enzymes, stimuli and signaling pathways. Nat Neurosci 13:1330–1337.
Rupaimoole R, Slack FJ (2017) MicroRNA therapeutics: towards a new era for the management of cancer and other diseases. Nat Rev Drug Discov 16: 203–222.
Schuettengruber B, Chourrout D, Vervoort M, Leblanc B, Cavalli G (2007) Genome regulation by polycomb and trithorax proteins. Cell 128:735–745.
Stathopulos PB, Li GY, Plevin MJ, Ames JB, Ikura M (2006) Stored Ca^{2+} depletion-induced oligomerization of stromal interaction molecule 1 (STIM1) via the EF-SAM region: an initiation mechanism for capacitive Ca^{2+} entry. J Biol Chem 281:35855–35862.
Tang B, Yang Y, Kang M, Wang Y, Wang Y, Bi Y, He S, Shimamoto F (2020) M(6)A demethylase ALKBH5 inhibits pancreatic cancer tumorigenesis by decreasing WIF-1 RNA methylation and mediating Wnt signaling. Mol Cancer 19:3.
Tao Y, et al. (2023) Epigenetic regulation of beta-endorphin synthesis in hypothalamic arcuate nucleus neurons modulates neuropathic pain in a rodent pain model. Nat Commun 14:7234.
Vos BP, Strassman AM, Maciewicz RJ (1994) Behavioral evidence of trigeminal neuropathic pain following chronic constriction injury to the rat's infraorbital nerve. J Neurosci 14:2708–2723.
Wan Z, Liu T, Wang L, Wang R, Zhang H (2020) MicroRNA-216a-3p promotes sorafenib sensitivity in hepatocellular carcinoma by downregulating MAPK14 expression. Aging 12:18192–18208.
Wang H, Wei Y, Pu Y, Jiang D, Jiang X, Zhang Y, Tao J (2019) Brain-derived neurotrophic factor stimulation of T-type Ca(2+) channels in sensory neurons contributes to increased peripheral pain sensitivity. Sci Signal 12:eaaw2300.
Wang Q, Zhang Y, Du Q, Zhao X, Wang W, Zhai Q, Xiang M (2023) SKF96365 impedes spinal glutamatergic transmission-mediated neuropathic allodynia. Korean J Physiol Pharmacol 27:39–48.
Wang H, Zhang M, Wei T, Zhou J, Zhang Y, Guo D (2021) Long non-coding RNA SNHG1 mediates neuronal damage in Parkinson's disease model cells by regulating miR-216a-3p/Bcl-2-associated X protein. Ann Transl Med 9:851.
Waxman SG, Zamponi GW (2014) Regulating excitability of peripheral afferents: emerging ion channel targets. Nat Neurosci 17:153–163.
Wei D, Mei Y, Xia J, Hu H (2017) Orai1 and Orai3 mediate store-operated calcium entry contributing to neuronal excitability in dorsal root ganglion neurons. Front Cell Neurosci 11:400.
Yang Z, Pan L, Liu S, Li F, Lv W, Shu Y, Dong P (2018) Inhibition of stromal-interacting molecule 1-mediated store-operated Ca(2+) entry as a novel strategy for the treatment of acquired imatinib-resistant gastrointestinal stromal tumors. Cancer Sci 109:2792–2800.
Yao Q, Chen Y, Zhou X (2019) The roles of microRNAs in epigenetic regulation. Curr Opin Chem Biol 51:11–17.
Zhang Y, Laumet G, Chen SR, Hittelman WN, Pan HL (2015) Pannexin-1 up-regulation in the dorsal root ganglion contributes to neuropathic pain development. J Biol Chem 290:14647–14655.
Zhang Y, Qian Z, Jiang D, Sun Y, Gao S, Jiang X, Wang H, Tao J (2021) Neuromedin B receptor stimulation of Cav3.2T-type Ca(2+) channels in primary sensory neurons mediates peripheral pain hypersensitivity. Theranostics 11:9342–9357.
Zhang Y, Qin W, Qian Z, Liu X, Wang H, Gong S, Sun YG, Snutch TP, Jiang X, Tao J (2014) Peripheral pain is enhanced by insulin-like growth factor 1 through a G protein-mediated stimulation of T-type calcium channels. Sci Signal 7:ra94.
Zhou Z, Mao M, Cai X, Zhu W, Sun J (2021) Store-operated calcium channels contribute to remifentanil-induced postoperative hyperalgesia via phosphorylation of CaMKIIalpha in rats. J Pain Res 14:3289–3299.